17

Fabrication and Applications of Microfiber

K. S. Lim[1], S. W. Harun[1,2], H. Arof[2] and H. Ahmad[1]
[1]*Photonic Research Center, University of Malaya, Kuala Lumpur,*
[2]*Department of Electrical Engineering, Faculty of Engineering, University of Malaya, Kuala Lumpur,*
Malaysia

1. Introduction

Microfibers have attracted growing interest recently especially in their fabrication methods and applications. This is due to a number of interesting optical properties of these devices, which can be used to develop low-cost, miniaturized and all-fiber based optical devices for various applications (Bilodeau et al., 1988; Birks and Li, 1992). For instance, many research efforts have focused on the development of microfiber based optical resonators that can serve as optical filters, which have many potential applications in optical communication and sensors. Of late, many microfiber structures have been reported such as microfiber loop resonator (MLR), microfiber coil resonator (MCR), microfiber knot resonator (MKR), reef knot microfiber resonator as an add/drop filter and etc. These devices are very sensitive to a change in the surrounding refractive index due to the large evanescent field that propagates outside the microfiber and thus they can find many applications in various optical sensors. The nonlinear properties of the micro/nanostructure inside the fiber can also be applied in fiber laser applications. This chapter thoroughly describes on the fabrication of microfibers and its structures such as MLR, MCR and MKR. A variety of applications of these structures will also be presented in this chapter.

2. Fabrication of microfiber

2.1 Flame brushing technique

Flame brushing technique (Bilodeau et al., 1988) is commonly used for the fabrication of fiber couplers and tapered fibers. It is also chosen in this research due to its high flexibility in controlling the flame movement, fiber stretching length and speed. The dimension of the tapered fiber or microfiber can be fabricated with good accuracy and reproducibility. Most importantly, this technique enables fabrication of biconical tapered fibers which both ends of the tapered fiber are connected to single-mode fiber (SMF). These biconical tapered fibers can be used to fabricate low-loss microfiber based devices.

Fig.1 shows a schematic illustration of tapered fiber fabrication based on flame brushing technique. As shown in Fig. 1, coating length of several cm is removed from the SMF prior to the fabrication of tapered fiber. Then the SMF is placed horizontally on the translation stage and held by two fiber holders. During the tapering, the torch moves and heats along the uncoated segment of fiber while it is being stretched. The moving torch provides a uniform heat to the fiber and the tapered fiber is produced with good uniformity along the

heat region. To monitor the transmission spectrum of the microfiber during the fabrication, amplified spontaneous emission (ASE) source from an Erbium-doped fiber amplifier (EDFA) is injected into one end of the SMF while the other end is connected to the optical spectrum analyzer (OSA). Fig. 2(a) shows diameter variation of the biconical tapered fiber fabricated using the fiber tapering rig while Fig. 2(b) shows the optical microscope image of the tapered fiber with a waist diameter of 1.7μm. With proper tapering parameters, the taper waist diameter can be narrowed down to ~800nm as shown in Fig. 2(c).

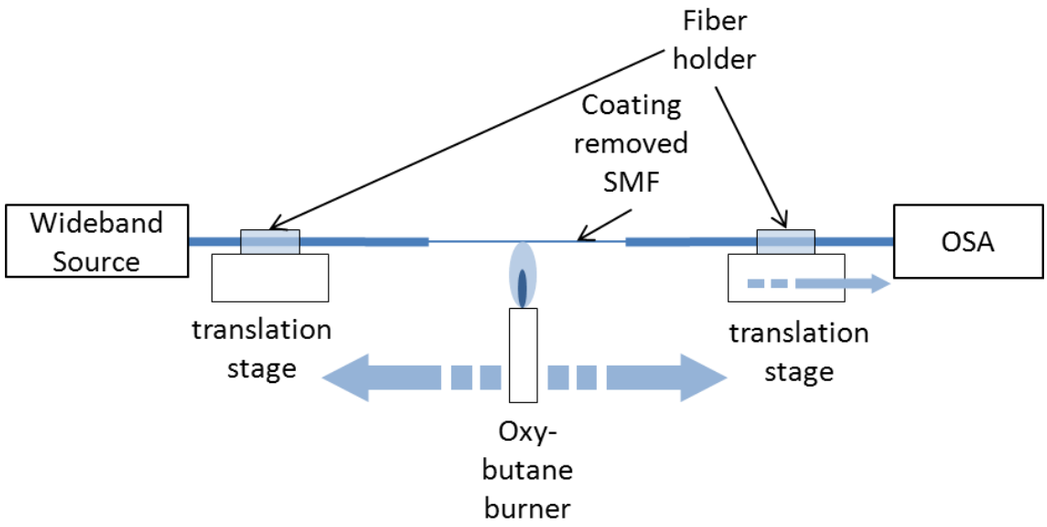

Fig. 1. Tapered fiber fabrication using flame brushing technique.

Adiabaticity is one of the important criteria in fabricating good quality tapered fibers. It is commonly known that some tapered fibers suffer loss of power when the fundamental mode couples to the higher order modes. Some fraction of power from higher order modes that survives propagating through the tapered fiber may recombine and interfere with fundamental mode. This phenomenon can be seen as interference between fundamental mode HE_{11} and its closest higher order mode HE_{12}. This results to a transmission spectrum with irregular fringes as shown by the dotted graph in Fig. 3 and the excess loss of the tapered fiber is ~0.6dB (Ding et al., 2010; Orucevic et al., 2007). This tapered fiber is not suitable to be used in the ensuing fabrication of microfiber devices. The solid curve in the same figure shows the transmission of a low loss tapered fiber with approximately more than 4mm transition length and the insertion loss lower than 0.3dB. Some analysis suggests that the coupling from fundamental mode to higher order modes can be minimized by optimizing shape of the tapers. In practice, adiabaticity can be easily achieved by using sufficiently slow diameter reduction rate when drawing tapered fibers or in other words manufacture tapered fibers with sufficiently long taper transition length. A detail discussion on the adiabatic criteria and optimal shapes for tapered fiber will be presented in the next section.

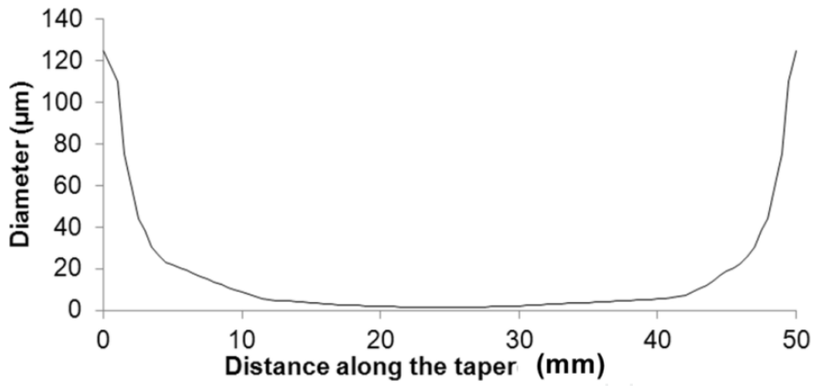

(a)

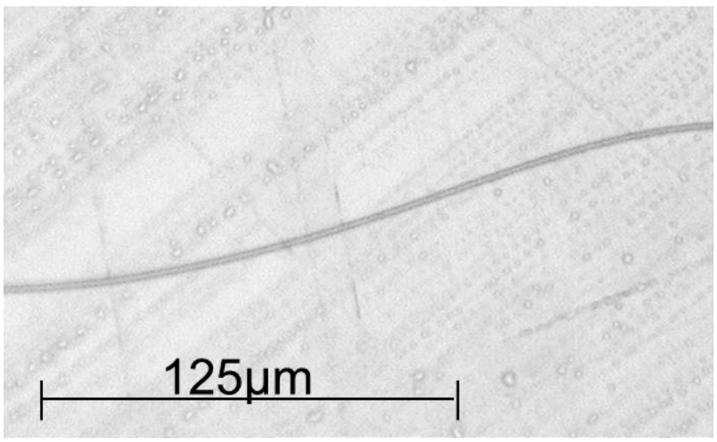

(b)

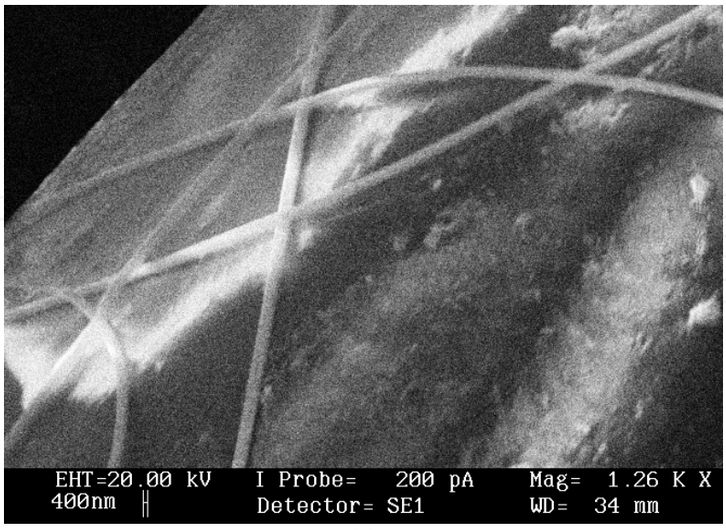

(c)

Fig. 2. (a)The diameter variation of a biconical tapered fiber fabricated in the laboratory (b) Optical microscope image of tapered fiber with a waist diameter of 1.7 µm (c) SEM image of a ~700nm waist diameter tapered fiber.

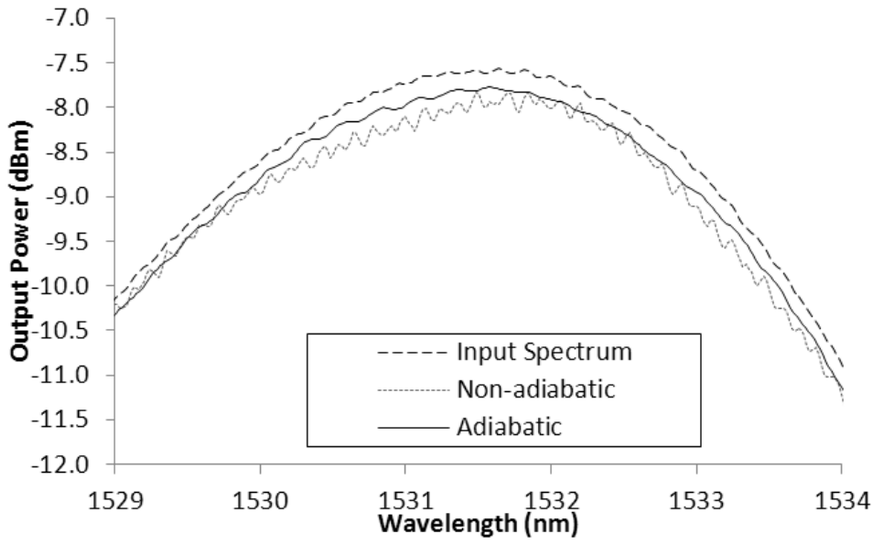

Fig. 3. Output spectra from a microfiber with 10 cm long and ~3μm waist diameter. Input spectrum from EDFA (dashed), adiabatic taper (solid) and non-adiabatic taper (dotted).

2.2 Adiabaticity criteria

Tapered fiber is fabricated by stretching a heated conventional single-mode fiber (SMF) to form a structure of reducing core diameter. As shown in Fig. 4, the smallest diameter part of the tapered fiber is called waist. Between the uniform unstretched SMF and waist are the transition regions whose diameters of the cladding and core are decreasing from rated size of SMF down to the order micrometer or even nanometer. As the wave propagate through the transition regions, the field distribution varies with the change of core and cladding diameters along the way. Associated with the rate of diameter change of any local cross section, the propagating wave may experience certain level of energy transfer from the fundamental mode to a closest few higher order modes which are most likely to be lost. The accumulation of this energy transfer along the tapered fiber may result to a substantial loss of throughput. This excess loss can be minimized if the shape of the fabricated tapered fiber follows the adiabaticity criteria everywhere along the tapered fiber (Birks and Li, 1992; Love et al., 1991).

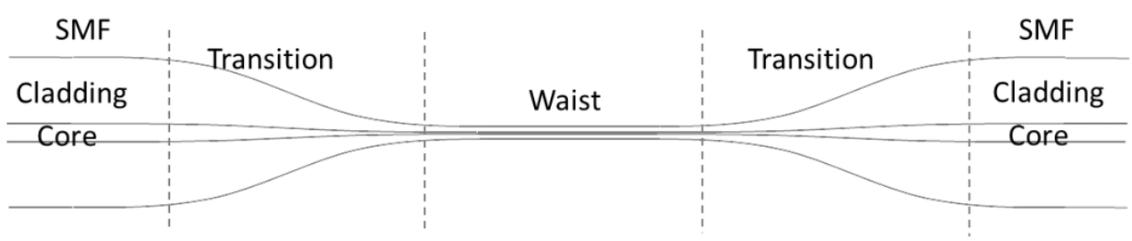

Fig. 4. Typical diameter profile of a tapered fiber.

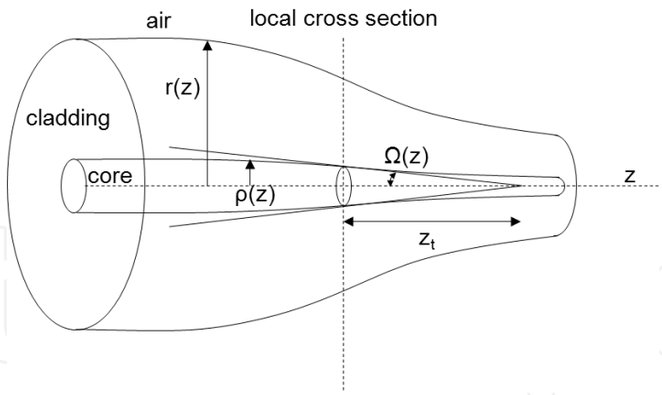

Fig. 5. Illustration of the taper transition.

Fig. 5 gives an illustration of a tapered fiber with decreasing radius where z denotes the position along the tapered fiber. Theoretically, an adiabatic tapered fiber is based on the condition that the beat length between fundamental mode LP_{01} and second local mode is smaller than the local taper length-scale z_t.

$$z_b > z_t \tag{1}$$

Referring to illustration in Fig. 5, z_t is given by

$$z_t = \rho / \tan\Omega \tag{2}$$

where $\rho = \rho(z)$ is the local core radius and $\Omega = \Omega(z)$ is the local taper angle.
The beat length between two modes is expressed as

$$z_b = \frac{2\pi}{\beta_1 - \beta_2} \tag{3}$$

where $\beta_1 = \beta_1(r)$ and $\beta_2 = \beta_2(r)$ are the propagation constants of fundamental mode and second local mode respectively. From the above equations, Inequality (1) can be derived to

$$\left|\frac{d\rho}{dz}\right| = \tan\Omega < \frac{\rho(\beta_1 - \beta_2)}{2\pi} \tag{4}$$

where $\frac{d\rho}{dz}$ is the rate of change of local core radius and its magnitude is equivalent to $\tan\Omega$.
For the convenience of usage and analysis, Inequality (4) is rewritten as a function of local cladding radius r=r(z),

$$\left|\frac{dr}{dz}\right| < \frac{r(\beta_1 - \beta_2)}{2\pi} \tag{5}$$

Based on this condition, adiabatic tapered fiber can be acquired by tapering a fiber at a smaller reduction rate in diameter but this will result to a longer transition length. Considering practical limitations in the fabrication of fiber couplers or microfiber based devices, long tapered fiber may aggravate the difficulty in fabrication. For the purpose of

miniaturization, short tapered fiber is preferable. To achieve balance between taper length and diameter reduction rate, a factor *f* is introduced to Inequality (5) and yields

$$\frac{dr}{dz} = -\frac{fr(\beta_1 - \beta_2)}{2\pi} \tag{6}$$

where the value of *f* can be chosen between 0 to 1. Optimal profile is achieved when *f* = 1. Practically, tapered fiber with negligibly loss can be achieved with *f* = 0.5 but the transition length of the tapered fiber is 2 times longer than that of the optimal tapered fiber.

2.3 Shape of tapered fiber

When a glass element is heated, there is a small increment in the volume under the effect of thermal expansion. However, the change in volume is negligibly small not to mention that the volume expansion wears off immediately after the heat is dissipated from the mass. It is reasonable to assume that the total volume of the heated fiber is conserved throughout the entire tapering process. Based on this explanation, when a heated glass fiber is stretched, the waist diameter of the fiber is reduced. The calculation of varying waist diameter and length of extension can be made based on the idea of 'conservation of volume'. Birks and Li (1992) presented simple mathematical equations to describe the relationship between shapes of tapered fiber, elongation distance and hot-zone length. Any specific shape of tapered fiber can be controlled by manipulating these parameters in the tapering process. The differential equation that describes the shape of the taper is given by

$$\frac{dr}{dx} = -\frac{r}{2L} \tag{7}$$

where *L* denotes the hot-zone length and r denotes the waist diameter.
The function of radius profile is given by the integral

$$r(x) = r_0 \exp\left(-\frac{1}{2}\int \frac{dx}{L}\right) \tag{8}$$

To relate the varying hot-zone length *L* with the elongation distance *x* during the tapering process, *L* can be replaced with any function of *x*. Linear function

$$L(x) = L_o + \alpha x \tag{9}$$

makes a convenient function for the integral in Eqn (8).

$$r(x) = r_0\left(1 + \frac{\alpha x}{L_0}\right)^{-1/2\alpha} \tag{10}$$

where r_0 denotes the initial radius of the fiber. To express the taper profile as a function of *z*, distance along the tapered fiber is given as;

$$r(z) = r_0\left(1 + \frac{2\alpha z}{(1-\alpha)L_0}\right)^{-1/2\alpha} \tag{11}$$

By manipulating the value of α, several shapes of tapered fiber can be produced such as reciprocal curve, decaying-exponential, linear and concave curve. Several examples of calculated taper shape based on different values of α can be found in the literature of (Birks and Li, 1992). Consider the case of tapered fiber with decaying-exponential profile as shown in Fig. 6, the fabrication of such tapered fiber requires a constant hot-zone length (α=0). From the theoretical model presented above, the function for the decaying-exponential profile is given by

$$r(z) = r_0 \exp(-z / L_0) \tag{12}$$

Based on this profile function, narrower taper waist can be achieved by using a small hot-zone length in the fabrication or drawing the taper for a longer elongation distance. Tapered fiber with a short transition length can be achieved from reciprocal curve profile based on positive value of α particularly with $\alpha = 0.5$.

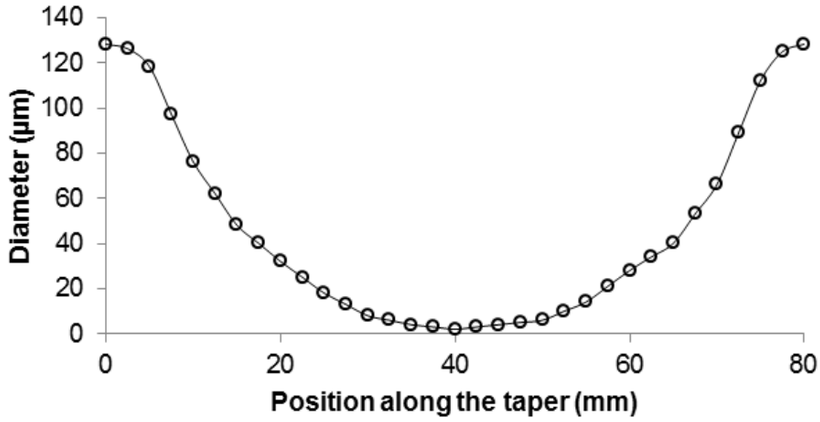

Fig. 6. A tapered fiber with decaying-exponential profile fabricated using a constant hot-zone L_0=10mm.

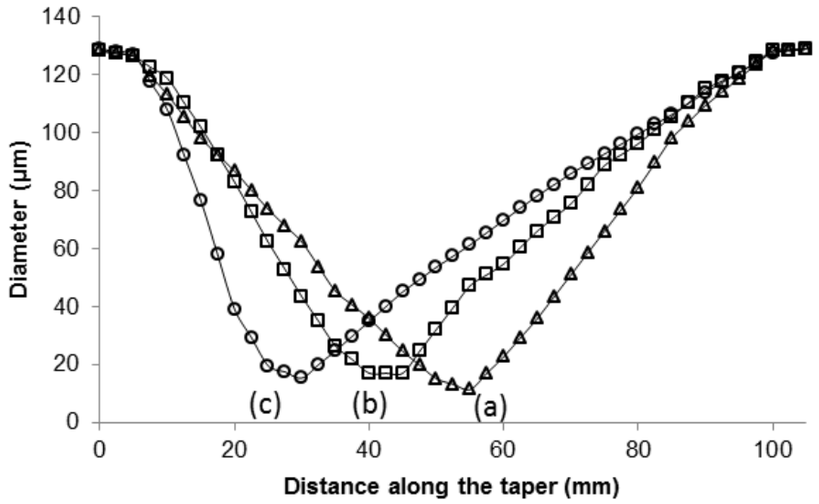

Fig. 7. Three linear taper profiles (a-c) with its smallest waist point at different positions on the tapered fibers. Profile (a) has its smallest waist point at the center of the tapered fiber.

Linear taper profile can be produced using α = -0.5 and the profile function is given by

$$r(z) = r_0\left(1 - \frac{2z}{3L_0}\right) \tag{13}$$

Fig. 7 shows typical examples of linear taper profiles. As shown in the figure, profile (a) has the smallest waist diameter, which located at the center of the tapered fiber. By doing some simple modification on the tapering process, the smallest waist point can be shifted away from the center to one side of the tapered fiber as shown by profiles (b) and (c) in Fig. 7. These profiles are found useful in the fabrication of wideband chirped fiber bragg grating, in which the grating is written on the transition of the tapered fiber. Long linear shape tapers make good candidates for the fabrication of such devices (Frazão and et al., 2005; Mora et al., 2004; Ngo et al., 2003; Zhang et al., 2003). On the other hand, linear profile tapers can be used for optical tweezing because of its capability to converge the optical wave to a high intensity at the taper tip (Liu et al., 2006; Xu et al., 2006). Microscopic objects are attracted to the high intensity field driven by the large gradient force at the taper tip. Fig. 8 gives a good example of such tapered fiber with 15cm linear taper profile. It was produced by using a long initial hot zone length L_o = 7cm and long elongation distance.

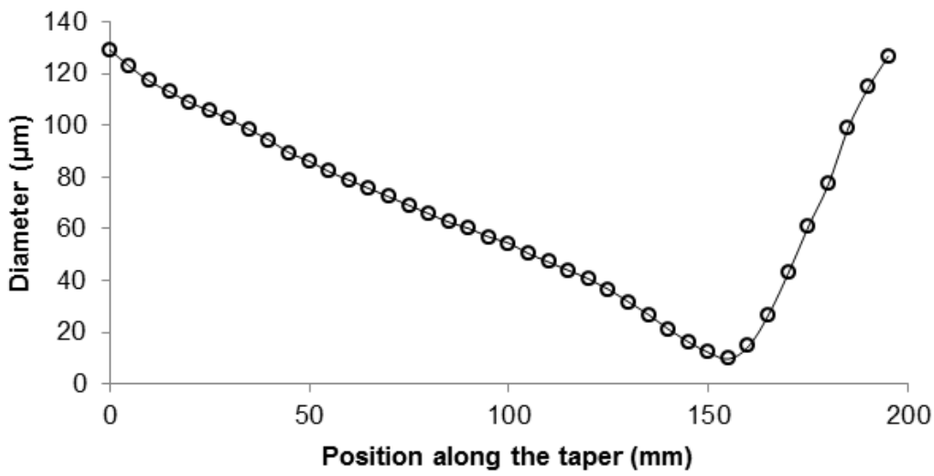

Fig. 8. The diameter of tapered fiber is linearly decreasing from ~128μm to ~10μm along the 15cm transition.

2.4 Throughput power of a degrading tapered fiber

In the high humidity environment, the concentration of water molecules in the air is high and very 'hazardous' to tapered fibers/microfiber. The increasing deposition of particles (dust) and water molecules on the microfiber is one of the major factors which causes adsorption and scattering of light that lead to perpetual decay in transmission (Ding et al., 2010). In an unprotected environment, freestanding microfibers may sway in the air due to the air turbulence. A small mechanical strength induced can cause cracks in the glass structure which may result to an unrecoverable loss in the microfibers (Brambilla et al., 2006).

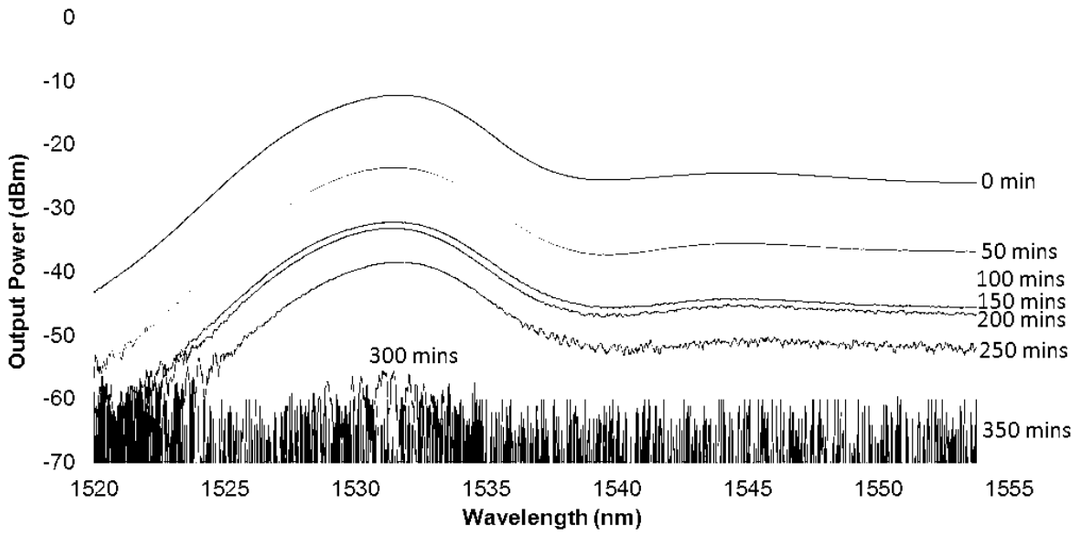

Fig. 9. The throughput power of the 10 cm long and ~3um diameter tapered fiber degrades over time.

Fig. 9 shows the output spectra of a tapered fiber in an unprotected environment. After the tapered fiber was drawn, it was left hanging in an open air and transmission spectrum was scanned and recorded every 50mins as presented in Fig. 9. Over the time, the deposition of dust and water molecules on the taper waist accumulated and the insertion loss of the tapered fiber increased over time. The output power of the tapered fiber dropped monotonically and eventually the power has gone too low beyond detection after 350mins. The throughput of the tapered fiber can be recovered by flame-brushing again as suggested in (Brambilla et al., 2006) but there is a risk that the tapered fiber can be broken after several times of flame-brushing and this solution is not practical. Despite the fact that the experiment was carried out in an air-conditioned lab where the humidity was lower (40-60%) but it was still too high for the tapered fibers. Besides, free standing tapered fibers are vulnerable to air turbulence or any sharp objects. New strategies for handling these tapered fibers are crucial for the ensuing research and fabrication of microfiber devices. In order to achieve that, this research team has been motivated to devise a packaging method to address all the problems mentioned earlier which will be discussed in the next section.

3. Packaging of microfiber

3.1 Embedding microfiber photonic devices in the low-index material

Besides the fast aging of bared microfiber in the air, the portability is another issue encountered when the microfiber is required at a different location. Moving the fabrication rig to the desired location is one way of solving the problem but it is not practical. Without a proper technique, it is risky to remove the tapered fiber from the fiber tapering rig and deliver it intact to another location. Xu and Brambilla (2007) proposed a packaging technique by embedding microfiber coil resonators in a low-index material named Teflon. Microfiber or microfiber device can be coated with or embedded in Teflon by applying some Teflon resin in solution on them and leave the solution to dry for several ten minutes. The resin is solidified after the solvent has finished evaporating from the solution, the optical properties and mechanical properties of the microfiber devices can be well preserved in the

material for a very long time (Xu and Brambilla, 2007). Jung et al. (2010) had taken slightly different approach by embedding microfiber devices in a low-index UV-curable resin. The resin is solidified by curing it with UV-light. Here, the detail procedure of embedding a microfiber device in the low-index UV-curable resin is demonstrated.

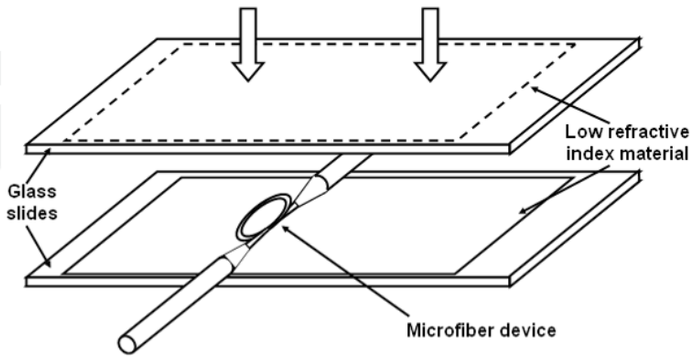

Fig. 10. Illustration of microfiber device embedded in a low refractive index material and sandwiched between two glass plates.

First, the assembled microfiber device is laid on an earlier prepared glass plate with a thin and flat layer of low refractive index material (UV-Opti-clad 1.36RCM from OPTEM Inc.) as shown in Fig. 10. The material has a refractive index of 1.36 at 1550nm. The thickness of the low refractive index material is approximately 0.5mm which is thick enough to prevent leakage of optical power from the microfiber to the glass plate. Some uncured resin is also applied on surrounding the microfiber device before it is sandwiched by another glass plate with the same low refractive index resin layer from the top. It is essentially important to ensure that minimum air bubbles and impurity are trapped around the fiber area between the two plates. This is to prevent refractive index non-uniformity in the surrounding of microfiber that may introduce loss to the system. During the tapering, coiling and coating processes, we monitored both the output spectrum and the insertion loss of the device in real time using the ASE source in conjunction with the OSA. The uncured resin is solidified by the UV light exposure for 3 ~7 minutes and the optical properties of the microfiber device are stabilized. The image of the end product is as shown in Fig. 11.

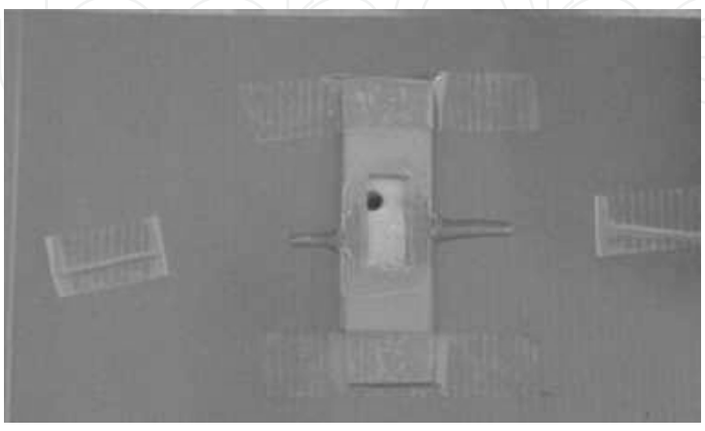

Fig. 11. The image of the end product of an embedded MLR in the low-index resin.

Fig. 12 shows recorded output spectra of the MKR at several intermediate times during the process of embedding it in a low-index UV-curable resin. The first spectrum in Fig. 12(a) was recorded right after an MKR was assembled. The fringes in the spectrum indicate that the resonance condition had been achieved in the MKR but the resonance extinction ratio remains appalling ~3dB. The MKR was benignly laid on an earlier prepared glass slide with thin layer of low refractive index material. After that, some low-index resin (refractive index ~1.36) in solution was applied onto the MKR by using a micropipette. Fig. 12(b) shows the stabilized output spectrum of the MKR and the improved resonance extinction ratio ~10dB. This phenomenon can be attributed to the reduction of index contrast; the mode field diameter (MFD) is the microfiber was expanded when it was immersed in the resin and the coupling efficiency of the MKR was altered. The changes of coupling coefficient and round-trip loss of the MKR may have induced critical coupling condition in the MKR and enhanced the resonance extinction ratio. At time = 4 minutes, UV-curing was initiated and a little bit of fluctuation is observed in the output power and extinction ratio (refer Fig. 12(c)) during the curing process. After UV-curing for 6 minutes, the output spectrum became very stable and the resin was finally solidified. Fig. 13 shows the optical microscope image of the embedded MKR in UV-curable resin.

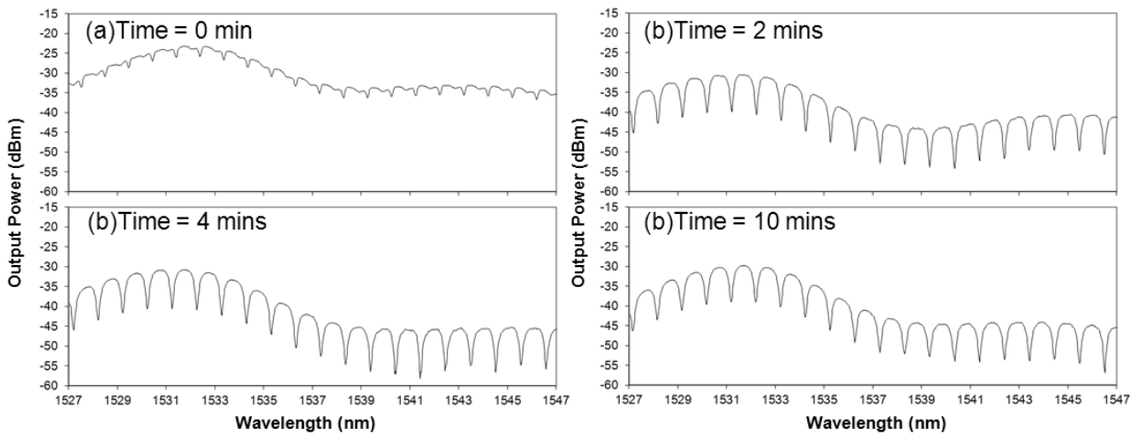

Fig. 12. Embedding an MKR in a low-index material. The time in each graph indicates when the output spectrum of the MKR is recorded. a) MKR is freestanding in the air b) some low-index resin applied on the MKR c) UV curing is initiated and d) resin is solidified.

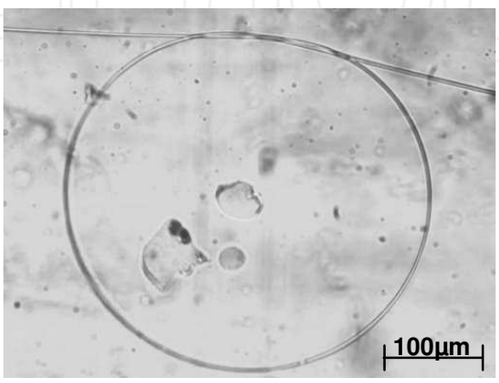

Fig. 13. Optical microscope image of an MKR embedded in UV-curable resin.

3.2 Packaging tapered fiber in a perspex case

Tapered fibers are susceptible to the air turbulence and the pollution of dust and moisture when exposed to air. It is very fragile when removed from the fiber tapering rig and maintaining the cleanliness of the tapered fiber in an unprotected condition is difficult. However, another simple packaging method had been devised to address all the difficulties mentioned. For the purpose of long term usage and ease of portability of the tapered fiber, a proper packaging process is essential. In the previous section, microfiber device is embedded in the low-index UV-curable resin to maintain the physical structure and resonance condition of the devices. Although, the refractive indices of the materials are in the range of 1.3~1.4 which is slightly lower than refractive index of silica tapered fiber and the mode can be still be confined within the tapered fiber but some optical properties such as numerical aperture (NA) and MFD will be altered due to the change in refractive index difference between silica microfiber and ambient medium when embedded in the low-index material. In the context of maintaining small confinement mode area and high optical nonlinearity, this method may not be a good idea.

In this section, a new packaging method is proposed where the tapered fiber is kept in a perspex case. The taper waist is kept straight and surrounded by the air without having any physical contact with any substance or object thus maintaining its optical properties in the air. The following part of this section provides detail descriptions of this packaging method. First, an earlier prepared perspex tapered fiber case which was made of several small perspex pieces with a thickness of 2.5mm was used in housing the tapered fiber. The perspex case mainly comprises of a lower part and upper part. Both parts of the perspex case were specially prepared in such a way that the benches at both ends of the perspex case were positioned exactly at the untapered parts of the tapered fiber. After a fresh tapered fiber was drawn, the lower part of the perspex case was carefully placed at the bottom and in parallel with the tapered fiber. That can done with the assistance of an additional translation stage. Then, the perspex case was slowly elevated upward until both benches touch both untapered parts of the tapered fiber as shown in Fig. 14(a). After that, some UV-curable optical adhesive (Norland Product, Inc) was applied to the untapered fibers that laid on the benches before the upper part of the tapered fiber case covered the tapered fiber from the top as shown in Fig. 14(b).

The UV-curable adhesive was used to adhere both the upper part and the lower part of fiber taper case. Despite that the refractive index of the optical adhesive(~1.54) is higher than silica glass (1.44) but the adhesive was only applied to untapered fiber and the light confined within the core of the fiber is unaffected. To cure the UV-curable adhesive, 9W mercury-vapour lamp that emits at ~254nm was used. Depending on the adhesive volume and its distance from the mercury-vapour lamp, the curing time takes for 2-8mins. After the adhesive was solidified and both case parts were strongly adhered to each other (Refer Fig. 14(c)). During the process illustrated in Fig. 14(a)-(c), the fiber taper was held by the two fiber holders in fiber taper rig and this helped to keep the fiber taper straight until the completion of the UV-curing process. After that the fiber taper and its case can be safely removed from the fiber holders. The fiber taper packaged inside the perspex case may remain straight permenantly. In the contrary, the fiber taper may suffer higher insertion loss if the taper fiber was bent during the packaging process. On the other hand, it is essential to prevent any physical contact between the taper waist with human hands or other objects.

The dust or moisture on the fiber taper may introduce loss to the transmission. In the final step, the perspex case was sealed by wrapping it with a piece of plastic wrap. This can minimize the pollution of dust or air moisture in the perspex case for a very long period of time. This fiber taper can be kept in storage for a week and possibly a fortnight without having an increment of loss more than 1.5dB however it is subject to taper dimension and its usage in the experiment.

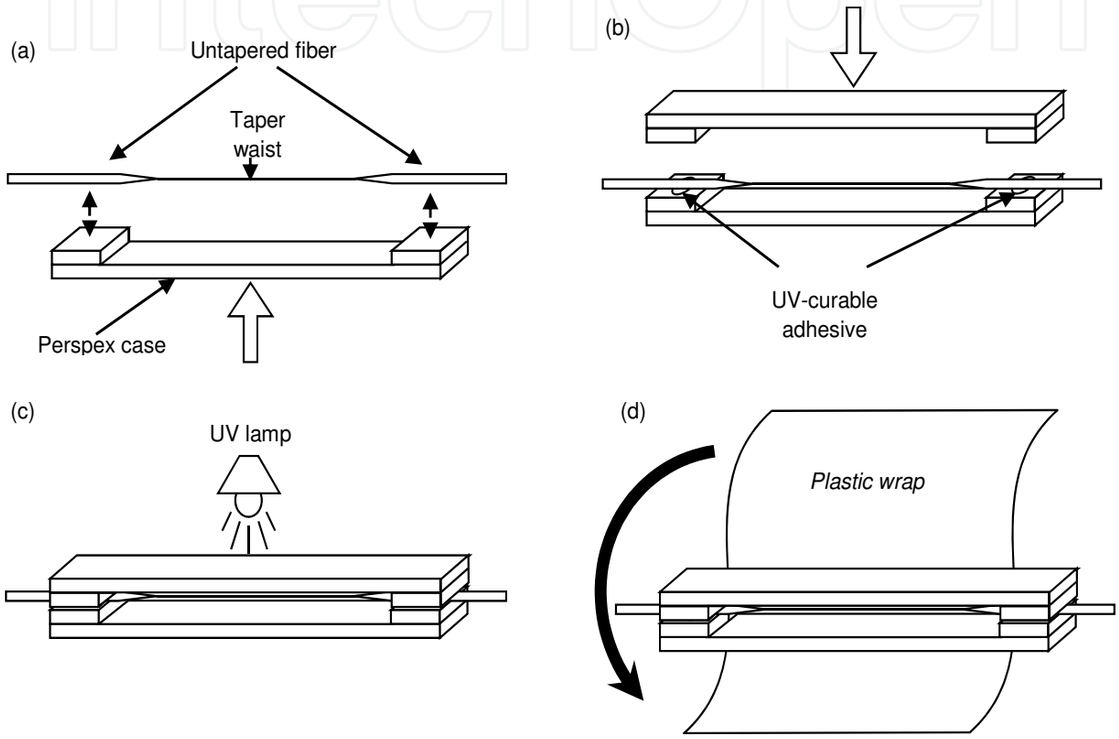

Fig. 14. Schematic illustration for tapered fiber packaging process.

To observe the characteristic of the tapered fiber as well as the reliability of the tapered fiber case over time, an observation on the transmission spectrum was conducted on the packaged tapered fiber for 6 days. Figs. 16(a) and (b) show the 6 days output spectra and output power observation, respectively for the packaged tapered fiber. Unlike the monotonic decrease in throughput power observed in Fig. 9(a), the curve of every transmission spectrum is closely overlaid to each other with a small power variation <1.2dB in the graph. Refer to Fig. 16(b), the variation of the total output power is spontaneous which can be attributed to the fluctuation of power at the ASE source and change of ambient temperature. In comparison with the taper fiber without packaging, obviously Perspex case plays its role well in preserving the tapered fiber to a longer lifespan; it enables portability and allows integration with more complex optical fiber configurations away from the fiber tapering rig.

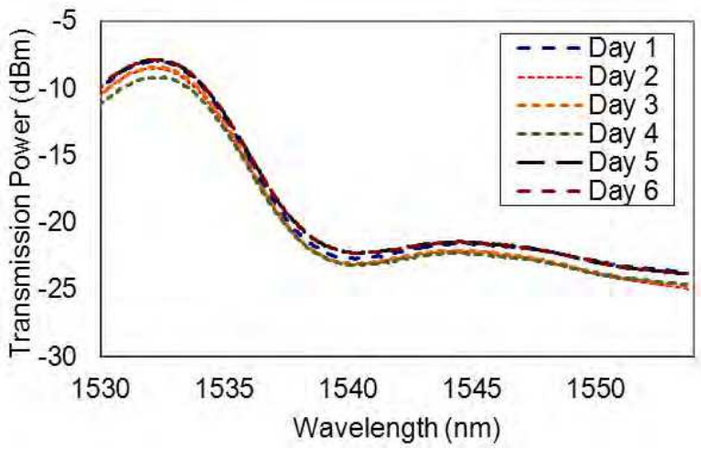

(a)

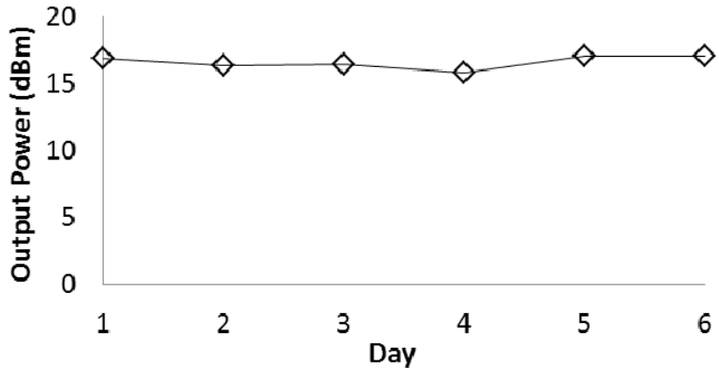

(b)

Fig. 16. The 6 days comparison of (a) output spectrum and (b) output power variation of the 10cm long and ~3um diameter tapered fiber packaged in perspex case.

4. Optical microfiber devices

Optical microfiber devices have attracted growing interest recently especially in their simple fabrication methods. This is due to a number of interesting optical properties in this device, which can be used to develop low-cost, miniaturized and all-fiber based optical devices for various applications (Guo et al., 2007). For instance, many research efforts have been focused on the development of microfiber/nanofibers based optical resonators that can serve as optical filters, which has many potential applications in optical communication, laser systems (Harun et al., 2010), and sensors (Hou et al., 2010; Sumetsky et al., 2006). Many photonic devices that are conventionally fabricated into lithographic planar waveguides can also be assembled from microfibers. Recently, there are many microfiber devices have been reported such as MLR (Harun et al., 2010; Sumetsky et al., 2005), MCR (Sumetsky, 2008; Sumetsky et al., 2010; Xu and Brambilla, 2007; Xu et al., 2007), MKR (Jiang et al., 2006; Lim et al., 2011; Wu et al., 2009), reef knot microfiber resonator as an add/drop

filter (Vienne et al., 2009) , microfiber mach-zehnder interferometer (MMZI) (Chen, 2010; Li and Tong, 2008) and etc. These microfiber based devices have the similar functionalities, characteristics and possibly the same miniaturizability with the lithographic planar waveguides. In future, these microfiber based devices may be used as building blocks for the larger and more complex photonic circuits. In this chapter, the transmission spectrum and the corresponding theoretical model of three microfiber based devices are presented, namely MLR, MKR and MMZI. In addition, some of the important optical properties of these devices will be reviewed and discussed.

4.1 Microfiber Loop Resonator (MLR)

MLRs are assembled from a single mode microfiber, which is obtained by heating and stretching a single mode fiber. In the past, many MLRs have been demonstrated. For instance and Bachus (1989) assembled a 2mm diameter MLR from an 8.5μm tapered fiber where the coupling efficiency can be compromised by the large thickness of the microfiber. However the deficiency was compensated by embedding the MLR in a silicone rubber which has lower and near to the refractive index of silica microfiber. The transmission spectrum with a frequency spectral range (FSR) of 30GHz is observed from the MLR (Caspar and Bachus, 1989). Later on, Sumetsky et al. had demonstrated the fabrication of MLR from a ~1μm diameter waist microfiber which has the highest achieved loaded Q-factor as high as 120,000 (Sumetsky et al., 2006). Guo et al. demonstrated wrapping a ~2 μm diameter microfiber loop around copper wire which is a high-loss optical medium. By manipulating the input-output fiber cross angle, the loss induced and the coupling parameter in the resonator can be varied. In the condition when the coupling ratio is equivalent to the round-trip attenuation, the MLR has achieved critical coupling and the transmission of resonance wavelength is minimum. In their work, critical coupling condition have been achieved which resonance extinction ratio as high as 30dB had been demonstrated (Guo et al., 2007; Guo and Tong, 2008).

4.1.1 Fabrication of MLR

Fig. 19 shows an example of ~3mm loop diameter MLR assembled from a ~2.0 μm waist diameter microfiber. Similar to other optical ring resonators, MLR has a 'ring' but manufactured from a single mode microfiber. This fabrication can be carried out with the assistance of two 3D translation stages as illustrated in Fig. 20. By aligning the three–axial position of each translation stage and twisting one of the pigtails, the microfiber is coiled into a loop. If the microfiber is sufficiently thin, the van der Waals attraction force between two adjacent microfibers is strong enough to withstand the elastic force from the bending microfiber and maintain the microfiber loop structure. The diameter of the loop can then be reduced by slowly pulling the two SMFs apart using the translation stages. Due the large evanescent field of the microfiber, a coupling region is established at the close contact between the two microfibers and a closed optical path is formed within the microfiber loop. Since the MLR is manufactured from an adiabatically stretched tapered fiber, it has smaller connection loss because microfiber based devices do not have the input-output coupling issue encountered in many lithographic planar waveguides. Despite the difference in the physical structure and fabrication technique between MLR and the conventional optical waveguide ring resonator, they share the same optical characteristics.

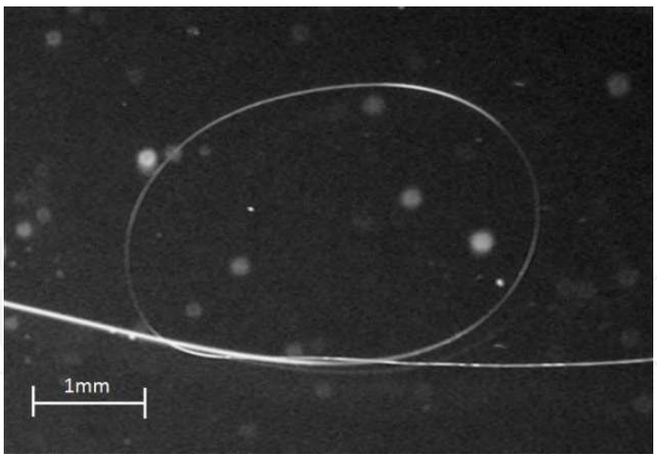

Fig. 19. Optical microscope image of an MLR.

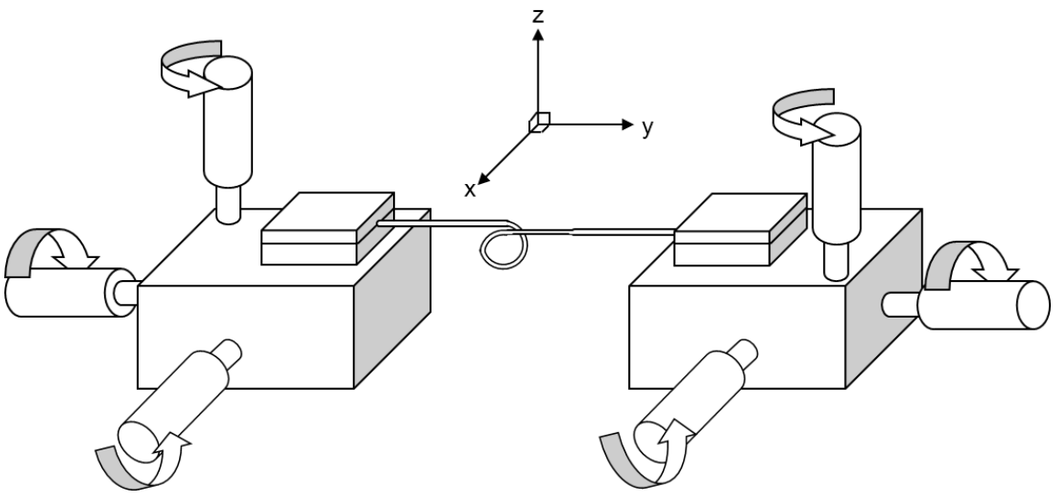

Fig. 20. Manufacture of MLR by using two three-dimensional stages.

4.1.2 Theory

The microfiber guides light as a single mode waveguide, with the evanescent field extending outside the microfiber. This evanescent field depends on the wavelength of operation, the diameter of the fiber and the surrounding medium. If the microfiber is coiled onto itself, the modes in the two different sections can overlap and couple to create a resonator. On every round-trip of light in the loop, there are fractions of light energy exchange between the two adjacent microfibers at the coupling region, the input light is allowed to oscillate in the closed loop and the resonance is strongest when a positive interference condition is fulfilled which can be related to this equation.

$$n\lambda_R = L \tag{14}$$

where L is the round-trip length, λ_R is the wavelength of the circulating waves and n is an integer. Positive interference occurs to those circulating waves and the wave intensity is building up within the microfiber loop. The relationship in Eqn (14) indicates that each

wavelength is uniformly spaced and periodic in frequency, a well-known characteristic of an optical multichannel filter. The amplitude transfer function for MLR is given as (Sumetsky et al., 2006);

$$T = \frac{\exp(-\alpha L/2)\exp(j\beta L) - \sin K}{1 - \exp(-\alpha L/2)\exp(j\beta L)\sin K} \tag{15}$$

sin$K$ denotes the coupling parameter where $K = \kappa l$, κ is the coupling coefficient and l is the coupling length. For every oscillation in the MLR, the circulating wave is experiencing some attenuation in intensity attributed to non-uniformity in microfiber diameter, material loss, impurity in the ambient of microfiber and bending loss along the microfiber loop. However, these losses can be combined and represented by a round-trip attenuation factor, exp(αL/2) in Eqn (15) while exp($j\beta L$) represents phase increment in a single round-trip in the resonator. The intensity transfer function is obtained by taking the magnitude squared of the amplitude transfer function in Eqn (15).

$$|T|^2 = \frac{\exp(-\alpha L) + \sin^2(K) - 2\exp(-\alpha L/2)\sin(K)\cos(\beta L)}{1 + \exp(-\alpha L)\sin^2(K) - 2\exp(-\alpha L/2)\sin(K)\cos(\beta L)} \tag{16}$$

The resonance condition occurs when

$$\beta L = 2m\pi \tag{17}$$

where m is any integer. The critical coupling occurs when

$$\sin K_c = \exp(-\alpha L/2) \tag{18}$$

The FSR is defined as the spacing between two adjacent resonance wavelengths in the transmission spectrum which is given by

$$\text{FSR, } \Delta\lambda \approx \frac{\lambda^2}{n_{eff} L} \tag{19}$$

or

$$\Delta\lambda \approx \frac{\lambda^2}{n_{eff}\pi D} \tag{20}$$

where D is the diameter of the circular loop.
In addition to the characteristic parameters mentioned earlier, Q-factor and finesse F are two important parameters that define the performance of the MLR. The Q-factor is defined as the ratio of resonance wavelength to the bandwidth of the resonance wavelength, the full wave at half maximum, FWHM (Refer Fig. 21). It is given as;

$$\text{Q} = \frac{\lambda}{FWHM} \tag{21}$$

The finesse is defined as the FSR of the resonator divided by the FWHM;

$$F = \frac{FSR}{FWHM} \tag{22}$$

Due to the narrow bandwidth at the resonance wavelengths, MLR also functions as a notch filter (Schwelb, 2004). The attenuation at the resonance wavelength can be used to filter out/drop the signal from specific channels in the WDM network by suppressing the signal power. In DWDM network, the spacing between two adjacent channels in the network is small therefore notch filter with narrow resonant bandwidth is preferable so that the signals from adjacent channels are unaffected by the attenuation in the drop channel. Based on the relationship in Eqn (22), narrow resonant bandwidth (FWHM) can be found in high finesse filter.

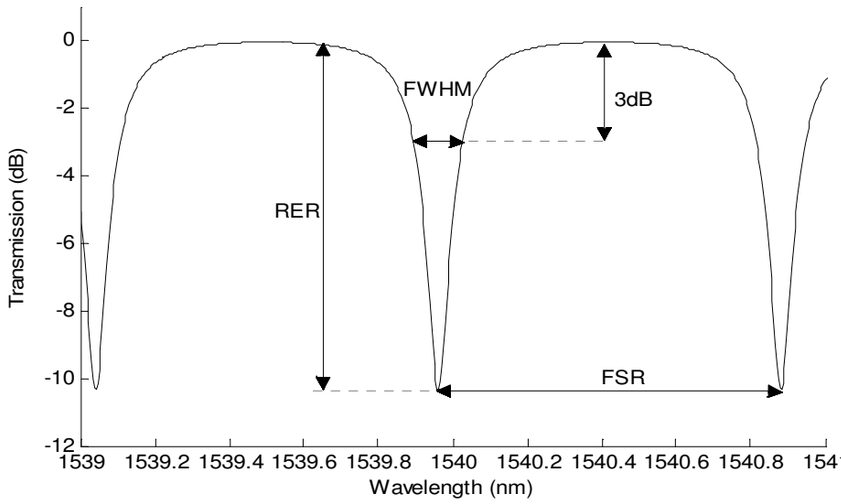

Fig. 21. Typical transmission spectrum of an MLR. The labels in the graph indicates the terminology used in the chapter. RER is an abbreviation for resonance extinction ratio.

4.1.3 Transmission spectra of MLRs

The typical transmission spectra of an MLR with different FSRs are shown in Fig. 22. For better clarity of viewing, the transmission spectra with different FSRs are presented in a increasing order from the top to the the bottom in the figure. These transmission spectra were recorded from a freestanding MLR in the air, started from a large loop diameter and the diameter is decreasing in step when the two microfiber arms of the MLR are stretched. Exploiting the van der Waals attraction force between the two microfibers in the coupling region, the resonance condition of the MLR can still be maintained during the stretching of microfiber. In the measurement, the loop diameters are at approximately 1.9mm, 1.4mm, 1.1mm, 0.8mm and 0.6mm which corresponds to FSR values of 0.275nm, 0.373nm, 0.493nm, 0.688nm and 0.925nm, respectively in the C-band region as shown in Fig. 22. These variations of FSR and loop diameter are very consistent with the reciprocal relationship expressed in Eqn (23). The loop diameter of an MLR is restricted by the microfiber elastic force, the smaller is the loop diameter the greater is the elastic force. Thus, it is difficult to keep the microfiber loop in shape when the loop diameter is very small and the MLR loses its resonance condition when the loop opens.

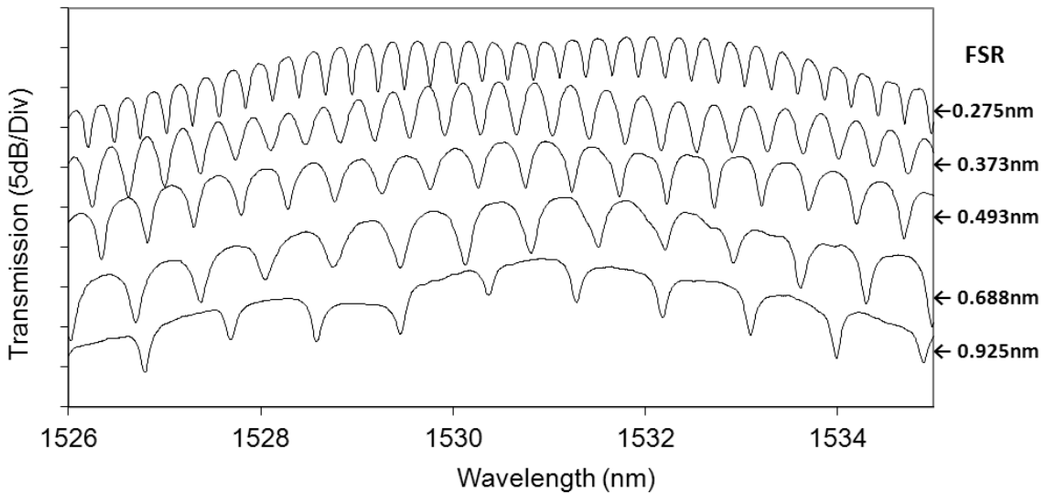

Fig. 22. Transmission Spectra of an MLR with increasing FSR (from top to bottom).

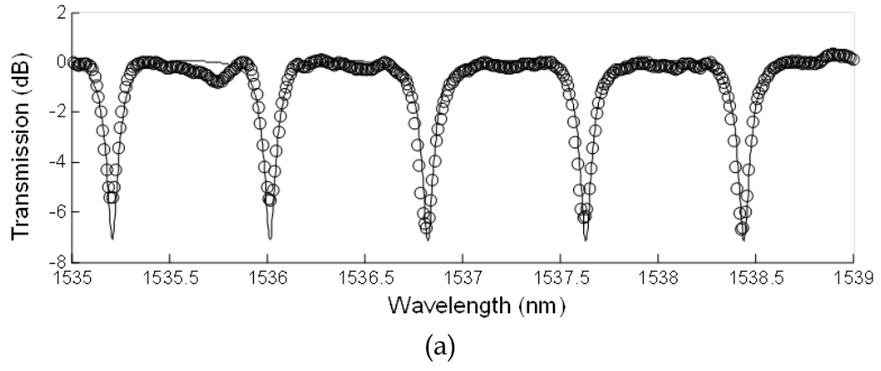

(a)

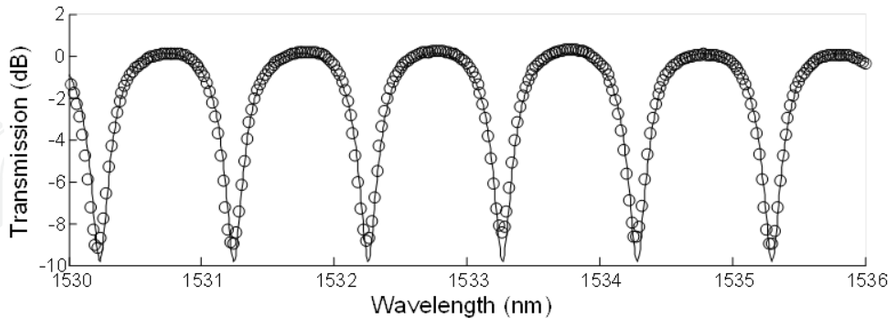

(b)

Fig. 23. The fitting of experimental data (circles) with the characteristic equation (solid line). (a) Q-factor ~18,000 and finesse ~9.5 (b) Q-factor ~5700 and finesse ~3.8

Fig. 23(a) and Fig. 23(b) show the fitting of experimental data with the (intensity) analytical model based on characteristic equation in Eqn (19). The best-fit parameters for the transmission spectrum in Fig. 23(a) are L = 2.03mm, exp (-aL/2) = 0.8853 and sin$K$ = 0.7354. The measured FSR ~0.805nm from transmission spectrum in Fig. 23(a) is in agreement with

the calculated FSR ~ 0.807nm. The bandwidth at the resonance wavelength, FWHM is ~0.085nm indicates that the Q-factor and finesse of the MLR are 18,000 and ~9.5. The best fit parameter for Fig. 23(b) are L = 1.61mm, sin K = 0.5133 and exp (-aL/2) = 0.6961. The measured FSR and FWHM are ~1.02nm and ~0.27nm respectively which indicate the values of Q-factor and finesse are ~5700 and ~3.8. In the comparison between the two spectra, the finesse provides a good representation in weighting the bandwidth between passband and stopband. The higher is the finesse the narrower is the stop-band compared with pass-band.

4.2 Microfiber Knot Resonator (MKR)

MKR is assembled by cutting a long and uniform tapered fiber into two. One tapered fiber is used for the fabrication of microfiber knot while the other one is used to collect the output power of the MKR by coupling the two tapered fiber ends and guides the output light back to an SMF. The fabrication of microfiber knot can be done by using tweezers. The coupling region of the MKR is enclosed by a dashed box in Fig. 24 where the two microfibers intertwisted and overlapped in the resonator. In comparison with MLR, MKR does not rely on van der Waals attraction force to maintain the coupling region yet it can achieve stronger coupling due to the rigid intertwisted microfibers structure at the coupling region. The knot structure can withstand strong elastic force of the microfiber and maintain a rigid resonator structure with a more stable resonance condition. Based on the same microfiber diameter, MKR of smaller knot diameter can be easily manufactured than that of MLR. However, MKR suffers a setback in a high insertion loss due to the cut-coil-couple process where the evanescent coupling between output microfiber and collector microfiber contributes a large fraction in the total insertion loss. The microfiber diameter in the range of 1~3μm is preferable because thinner microfiber is very fragile and it breaks easily in the fabrication of MKRs. Nonetheless, the operating principle of MKR is identical to MLR as it is based on self-touching configuration thus the same characteristic equation can be used to describe the transmission spectrum of MKR.

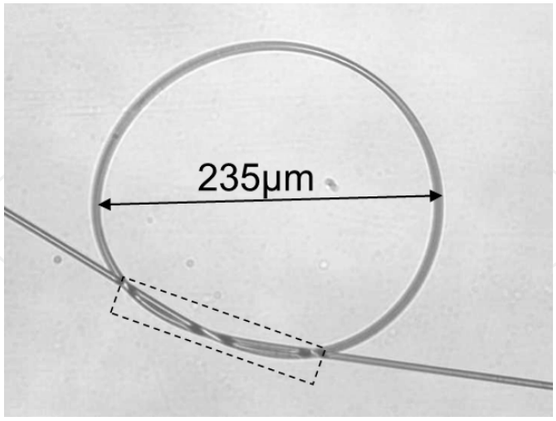

Fig. 24. Optical microscope image of an MKR.

4.2.1 Transmission spectra of MKRs

MKR offers better capability in achieving smaller knot diameter. The knot can withstand the strong elastic force of microfiber and it can achieve a small knot diameter that cannot be achieved in the MLR. Fig. 25 shows transmission spectra of an MKR assembled in the

laboratory. The transmission spectra are presented in an increasing order from the top to bottom of the figure and the values are 0.803nm, 1.030nm, 1.383nm, 1.693nm, 2.163nm and 2.660nm within the vicinity of 1530nm. The corresponding knot diameters are approximately 640μm, 500μm, 370μm, 310μm, 240μm and 190μm.

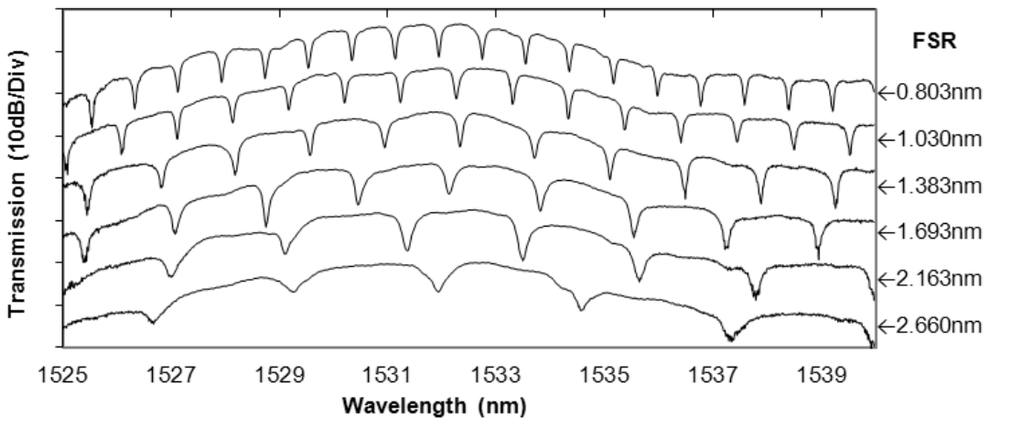

Fig. 25. Transmission Spectra of an MKR with increasing FSR (from top to bottom).

4.2.2 Resonance condition of microfiber knot resonator immersed in liquids

Recently, microfiber resonators are suggested in numerous applications particularly in the sensing applications (Lim et al., 2011; Sumetsky et al., 2006). The operating principles of these sensors rely on the characteristics of the resonance, the variation of the position of resonance wavelength and the resonance extinction ratio with the sensing parameters, temperature, refractive index and etc. (Wu et al., 2009; Xu et al., 2008). The resonance condition of a resonator relies on the index contrast between microfiber and its ambient medium, evanescent field strength and distance between two microfibers in the coupling region. Large evanescent field which can be found in thinner microfibers is one of the solutions to achieving higher coupling in microfiber resonators. The large fraction of light intensity in the evanescent field allows stronger mode interaction between two microfibers and yields high coupling coefficient. Caspar et al. suggest embedding the microfiber resonator into a medium that has a slightly lower refractive index than that of silica. Due to the small index contrast, the microfiber has a larger evanescent field which yields stronger coupling in the resonator (Caspar and Bachus, 1989; Xu and Brambilla, 2007). Besides being used as a post-fabrication remedy for improving the resonance condition of the resonator, embedding also offers good protection from the fast aging process and enabling portability for the microfiber devices. Vienne at el. have reported that when a microfiber resonator is embedded in low-index polymer, the optimal resonance wavelength is down-shifted by ~20% (Vienne et al., 2007). However, there is very few literatures that provide mathematically analysis on the effect of embedding in low index contrast medium to the resonance condition of the resonator. In order to achieve a better understanding, an experiment on an MKR immersed in liquid solutions was carried out. MKR was used in the experiment due to its rigid knot structure and strong interfiber coupling. The knot structure and resonance condition could be easily maintained during the immersing process.

Unlike MLR that exploits van der Waals attractive force to maintain the structure of the loop, MKR has a more rigid knot structure with interfiber twisted coupling. Nonetheless,

both MLR and MKR share the same optical properties, the same transmission equation can be used to describe both structures. Fabrication of an MKR started with fiber tapering using heat and pull technique. After a single-mode biconical tapered fiber was drawn, it was cut at one third part of the waist which the longer section of tapered fiber was used for the fabrication of knot by using tweezers. Then the second section was used as collector fiber by evanescent coupling (Tong et al., 2003) with the output port of the MKR. Immediately after that, the transmission spectrum of the freestanding MKR in the air was recorded by an OSA. After that, the MKR was embedded in propan-2-ol solution that has a refractive index (RI) of 1.37. First, the MKR was slowly laid horizontally on an earlier prepared flat platform deposited with a thin layer of propan-2-ol. Using a micropipette, a small volume of propan-2-ol solution was dropped onto the MKR and had it entirely immersed in the solution. The structure of the microfiber knot was intact and the resonance was maintained. This is the crucial part that distinguishes MKR from MLR. It is very difficult to maintain the loop structure and resonance of MLR when immersed in the liquid.

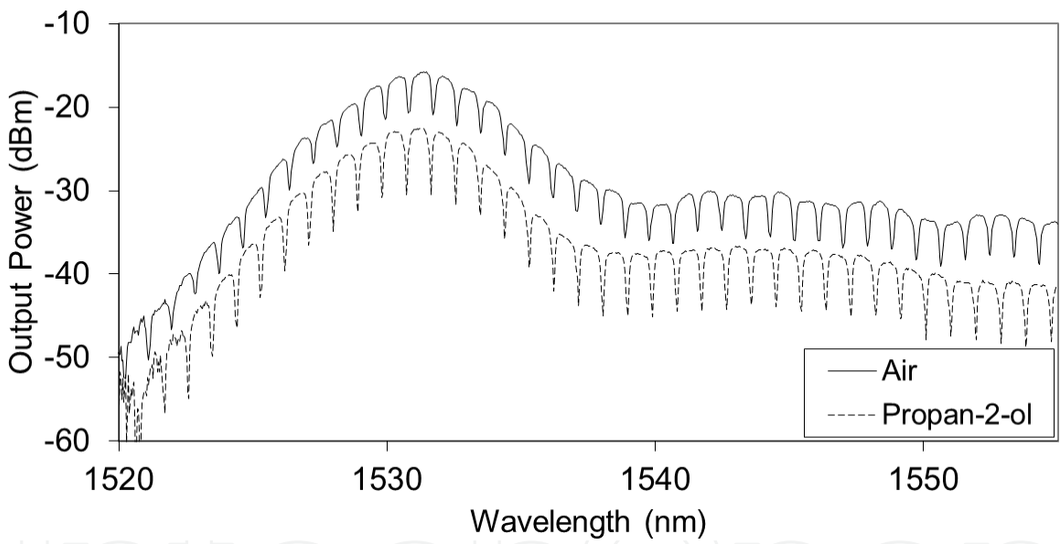

Fig. 26. The transmission spectra of MKR in the air (solid) and propan-2-ol solution (dashed).

Fig. 26 shows the overlaid transmission spectra of the MKR in the air (solid) and solution (dashed). Refering to the peak powers of both spectra, it is easy to determine that the MKR had suffered an additional ~7dB excess loss after it was immersed in the solution. The drop in coupling efficiency at the evanescent coupling between MKR output microfiber and collector microfiber constituted a large fraction in this excess loss. On the other hand, the resonance extinction ratio of the MKR had improved from ~5dB to ~8dB. In the analysis of resonance characteristics, the coupling parameter, $\sin\kappa\ell$ and round-trip attenuation factor of MKR, $\exp(-aL/2)$ can be extracted from the best-fit curves (lines) for the offset experimental data (circles) in Fig. 27(a) and Fig. 27(b) based on the transfer function in (18).

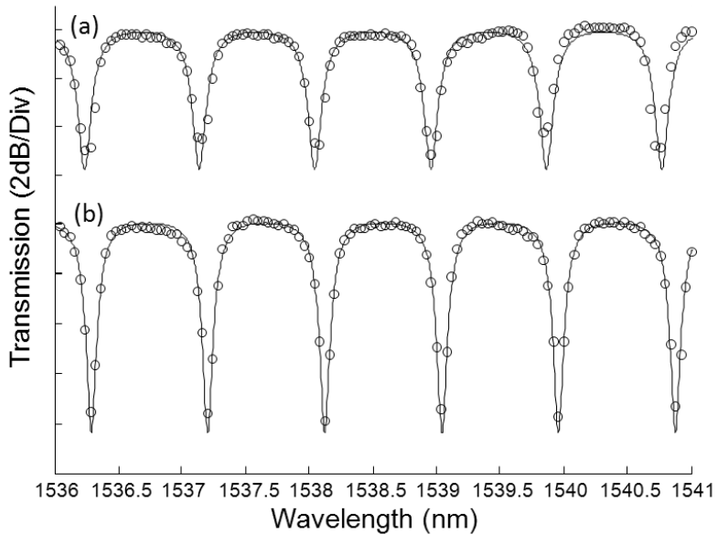

Fig. 27. The offset experimental data (circles) with its best fit curve (solid line) (a) air, RI ~1.00 (b) propan-2-ol, RI ~1.37.

In the air, the best fit parameters for the transmission spectrum in Fig. 27(a) are $\sin\kappa\ell$ = 0.6207 and $\exp(-aL/2)$= 0.8547. When the MKR was immersed in the propan-2-ol solution, the best fit parameters for Fig. 27(b) are $\sin\kappa\ell$ = 0.6762 and $\exp(-aL/2)$ = 0.8361. The reduction in round-trip attenuation factor can be attributed to the small index contrast between microfiber and ambient medium when immersed in the solution so that the bending loss at the microfiber knot is higher. The output - collector coupling loss is excluded from this analysis as it only affects the total output power (position in the vertical axis) and it can be eliminated in the offset spectrum. Based on Eqn (18), the resonance state of the resonator can be determined from the following expression

$$\delta = \left| \frac{\exp(-\alpha L/2) - \sin\kappa l}{1 - \exp(-\alpha L/2)\sin\kappa l} \right| \tag{23}$$

Smaller value of δ indicates that the state of resonance is closer to the critical coupling condition and it yields larger resonance extinction ratio. In fact, the resonance extinction ratio can be estimated by

$$RER \sim 20\log_{10}\delta \tag{24}$$

Comparing the two spectra, the spectrum in Fig. 27(b) has higher coupling and smaller round-trip attenuation factor which give smaller value in δ = 0.3679 if compared with δ = 0.5060 obtained from the spectr $\sin\kappa\ell$ and resulting the lower coupling value. The next experimental data may provide an example for such self-defeating scenario.The transmission spectra of an MKR in the air and low-index UV-curable resin (UV-Opti-clad 1.36RCM from OPTEM Inc.) with an RI of ~1.36 are as shown in Fig. 28(a) and Fig. 28(b) respectively. The coupling parameter, $\sin\kappa\ell$ had dropped from 0.7132 to 0.6247 when it was immersed in the water. On the other hand, the round-trip attenuation factor, $\exp(-aL/2)$ suffers greater fall from 0.9432 to 0.7538. In spite of that, the resonance extinction ratio had

increased from ~2dB to ~10dB. This is in agreement with the decreasing value of δ from 0.7027 to 0.2440 and the state of resonance is closer to critical coupling condition.

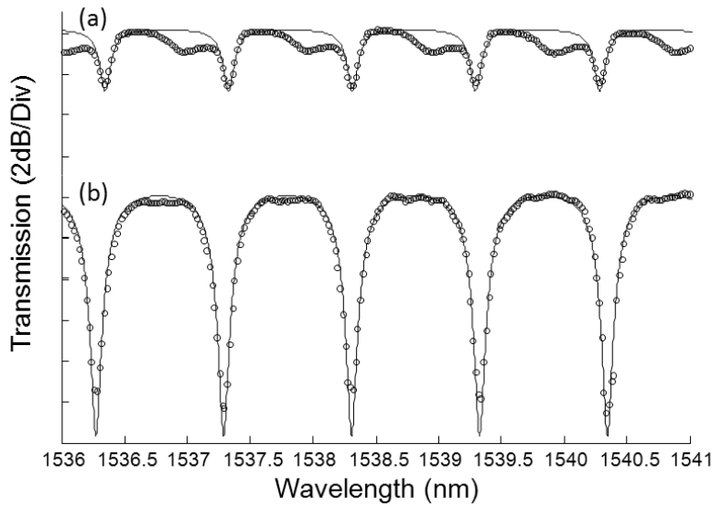

Fig. 28. The transmission spectra of MKR in different ambient mediums (a) air, RI ~1.00 (b) low-index resin, RI ~1.36.

Immersing MKR in a near-index medium do not always promise an improvement in the resonance condition or RER. There is a possibility that the changes in round-trip attenuation factor and coupling parameter yield larger value of δ and decreases the RER. Fig. 29 provides an example for this scenario. The best-fit parameter for the experimental data in the air (solid) are $\sin\kappa\ell$ = 0.6235 and $\exp(-aL/2)$ = 0.8145 respectively. After the MKR is immersed in the water (dashed), the values have varied to $\sin\kappa\ell$ = 0.7833 and $\exp(-aL/2)$ = 0.9339. In the air, the low value of round-trip attenuation factor can be attributed to the large amount of deposited dust on the microfiber surface which was introduced from the tweezers during the fabrication of microfiber knot. After it was immersed in the water, some portion of the dust might have been 'washed' away and that increases the round-trip attenuation factor. The value of δ has decreased from 0.3881 to 0.5609 which is an indication of the resonance state deviates from critical coupling.

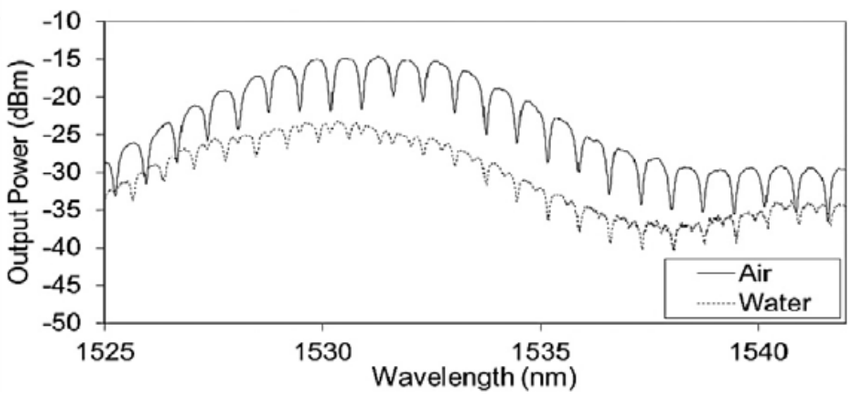

Fig. 29. Example of an MKR with decreased resonance extinction ratio after it is immersed in the water (RI ~1.33).

The purpose of using liquid solutions of different RIs is to investigate the influence of different index-contrasts to the resonance characteristics of the MKR. However, there was no significant indication observed in the experiment showing difference between the solutions. The only obvious changes were observed at the moment when the MKRs were immersed in the solutions. It is believed that the index contrasts induced by these three liquids are within a narrow range from 0.07 to 0.11 and the differences among them are too small to make significant impact on the characteristics of the MKR. On the other hand, we believe that that the microfiber waist diameter and orientation of the microfibers in the coupling region have an important relationship with the resonance of MKR. More investigations pertaining to those parameters are needed.

4.2.3 Polarization dependent characteristic

Microfiber based resonator exhibits strong dependence on its input polarization state. Similar characteristic was reported by Caspar et al. (Caspar and Bachus, 1989) where the extinction ratio of the resonator varies with the change of input state of polarization.

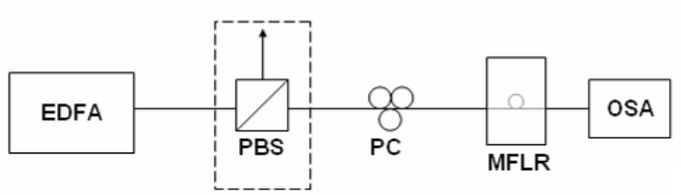

Fig. 30. Experimental set-up to investigate the polarization dependent characterıstıc of the MLR (Lim et al., 2011). Polarized wideband source from EDFA is acquired with the aid of PBS (Dashed box), an unpolarized wideband source can be obtained by removing PBS from the setup.

In the investigation of polarization state dependent characteristics, a simple experimental setup as shown in the Fig. 30 is established. First, the unpolarized ASE source from an EDFA was linearly polarized by a PBS, followed by a PC for controlling the state of polarization (SOP) of the polarized source before it was fed into the MLR. Fig. 31 shows the transmission spectra of the MKR at various resonance conditions of the MLR, which was obtained at different input wave SOP. Both spectra (i) in Fig. 31(a) and Fig. 31(b) show the transmission of the MLR based on an unpolarized input wave (without PBS), which resonance condition was unaffected by the adjustment of the PC. In contrast, the resonance condition for the MLR with polarized input wave was sensitive to the PC adjustment. By carefully adjusting the PC, the resonance extinction ratio could be enhanced or reduced as depicted in spectra (ii) and (iii) of both Fig. 31(a) and Fig. 31(b). Nevertheless, the wavelength of each peak and the FSR remained unchanged regardless of input wave SOP. It is appropriate to attribute this phenomenon to the polarization dependent coupling in the MLR where the interfiber coupling, twisting and alignment of microfiber in the coupling region are accounted for the coupling coefficient difference between two orthogonal polarization states (Bricheno and Baker, 1985; Chen and Burns, 1982; Yang and Chang, 1998). Associated with the coupling coefficient, the resonance extinction ratio of a microfiber based resonator can be improved by using an optimized polarized input light. However, more efforts are required for more in-depth study and to explore the possible applications in many fields such as multi-wavelength laser generation and sensing.

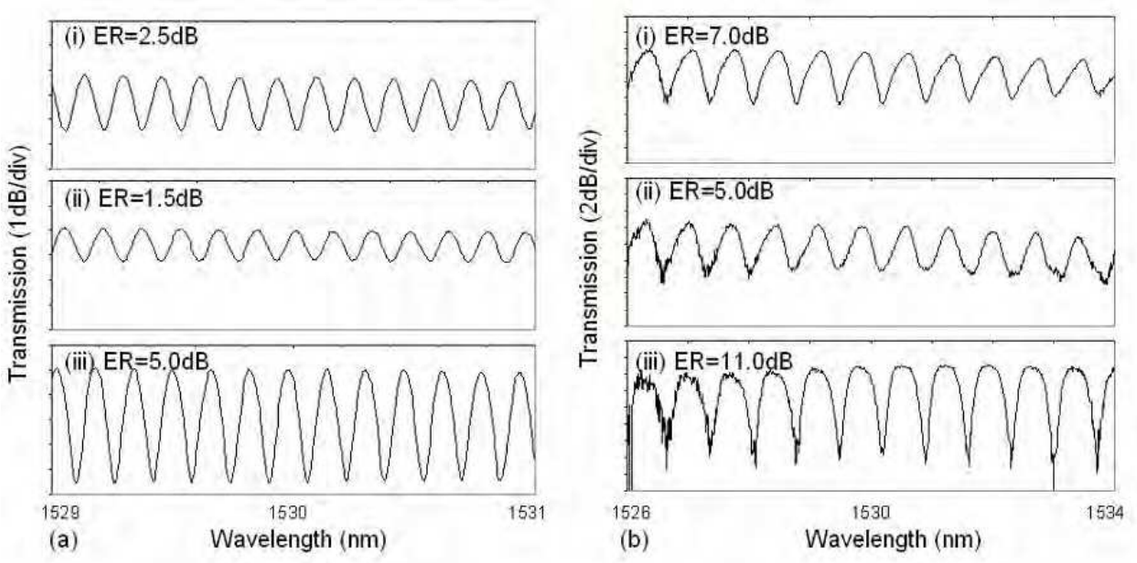

Fig. 31. The spectra of two MLRs for different input wave SOP. (a) FSR=0.162nm at 1530nm (b) FSR=0.71nm at 1530nm.

4.2.4 Thermal dependent characteristic

Microfiber based devices are very sensitive to variation of ambient temperature due to the strong dependence of the microfiber dimension and refractive index on temperature. In a thermally unstable environment, these devices may experience thermal drift in the transmission spectrum and fluctuation in the transmission power. However, this problem can be alleviated by the placing the devices in a temperature controlled housing (Dong et al., 2005). Sumetsky et al. demonstrated a MLR based ultrafast sensor for measurement of gas temperature. Taking advantage of the close contact between the MLR and air, the change in gas temperature in the ambient of MLR can be determined from the transmission power at the resonance wavelengths within a short response time of several microseconds (Sumetsky et al., 2006). Besides, the positions of resonance wavelengths are found to be sensitive to temperature change. The spectral shift of an MLR can be expressed in a linear function of temperature. The property enables temperature measurement based resonance wavelength shift with higher accuracy (Wu et al., 2009; Zeng et al., 2009).

MKRs exhibit the similar optical properties with MLRs. The free spectral range of MKR takes in the form of Eqn (22). Based on this equation, the variations in effective index n_{eff} and round-trip length L may lead to transmission spectral shift and their relationship can be expressed as

$$\frac{\Delta\lambda_{res}}{\lambda_{res}} = \left(\frac{\Delta n_{eff}}{n_{eff}} + \frac{\Delta L}{L} \right)_{Temp.} \tag{25}$$

In relation with temperature, both terms on the right hand side of Eqn (25) expresses two linear thermal coefficients; thermal-optic coefficient (TOC) and thermal expansion coefficient (TEC) [13]. With this interpretation, Eqn (25) can be rewritten as

$$\frac{\Delta\lambda_{res}}{\lambda_{res}} = (\alpha_{TOC} + \alpha_{TEC})\Delta T \tag{26}$$

Fig. 32(a) shows the transmission spectra of MKR at temperatures of 30°C, 35°C and 40°C. The spectral shift is approximately 26pm for every temperature increment of 5°C and the linearity between wavelength shift and temperature change can be seen from the linear fitting of experimental data in Fig. 32(b).

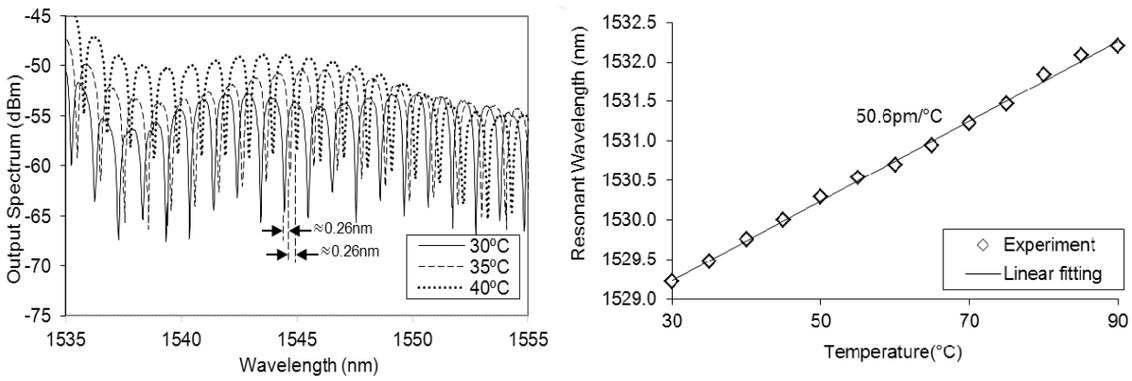

(a) (b)

Fig. 32. (a) The output spectra of an MKR at temperature of 30°C(solid), 35°C(dashed) and 40°C (dotted) (b) The temperature response of the MKR has spectral sensitivity of 50.6pm/°C.

This characteristic has opened up new possibilities for temperature sensing and spectral control based on temperature manipulation. It provides a solution for stabilizing the spectrum of the device which often affected by the thermal drift. Dynamic spectral shift in optical filter can be realized by exploiting this characteristic. In addition, the insusceptibility of fiber-optic components to electrical noise has made these devices very attractive for many industrial sensing applications.

4.2.5 Microfiber knot resonator based current sensor

A variety of fiber optic based current sensors have been investigated in recent years using mainly a single mode fiber (SMF) of clad silica. They are typically divided into two categories, where one is based on Faraday Effect and the other is based on thermal effect. The former is capable to remotely measure electrical currents, but the device requires a long fiber due to the extremely small Verdet constant of silica. The latter needs a short length of fiber but requires complex manufacturing techniques to coat fibers with the metals. Recently, a resonant wavelength of the MLR has been experimentally reported to shift with electric current applied to the loop through a copper rod. An acceptable transmission loss is achieved despite the fact that copper is not a good low-index material to support the operation of such structure (Guo et al., 2007). This finding has opened up a way to enable dynamic and efficient spectrum control for optical filters by manipulating an electric current dependence spectral shift characteristic of the microfiber based resonator. Microfiber based devices have a strong dependence on temperature due to the thermal expansion characteristic and thermo-optic effect of silica glass. As discussed earlier in Section 12, the transmission spectrum of a microfiber based device shifts as the ambient temperature varies

and the relationship between these two variables is well described by the linear equation in Eqn. (26).

In this section, spectral tunable MKR is demonstrated based on the idea of thermally induced resonant wavelength shift. By manipulating the applying electric current through the microfiber knot wrapped copper wire, the copper wire acts as a heating element and induces temperature change in the MKR. The transmission spectrum of the MKR shifts corresponds to the temperature change. These modified MKRs can be used as low-cost and fast response tunable optical filters which are useful in the applications of optical signal processing, WDM communication and etc. On the other hand, this opto-electrical configuration may operate as a dynamic current sensor with strong immunity to electric noise. In addition, it has a dynamic operational range extending to the regime of extreme high temperature or pressure.

Fabrication

First, a ~2μm diameter silica microfiber is fabricated from a SMF using flame-brushing method (Graf et al., 2009). Then the microfiber is cut and separated into two unequal parts in which the longer one is used in the knot fabrication and the other one is used as a collector fiber to collect the transmitted light from the MKR (Jiang et al., 2006). During the fabrication of the knot, the copper wire is inserted into the knot which diameter is bigger than the diameter of the copper wire (Refer Fig. 33(a)). The light path from the knot resonator is completed by coupling the two microfiber ends. At least ~3 mm of coupling length between two microfibers is required to achieve strong van der Waal attraction force to keep them attached together. The microfiber knot diameter is then reduced and fastened on the copper wire by pulling microfibers from both arms of the microfiber knot as illustrated in Fig. 33(b).

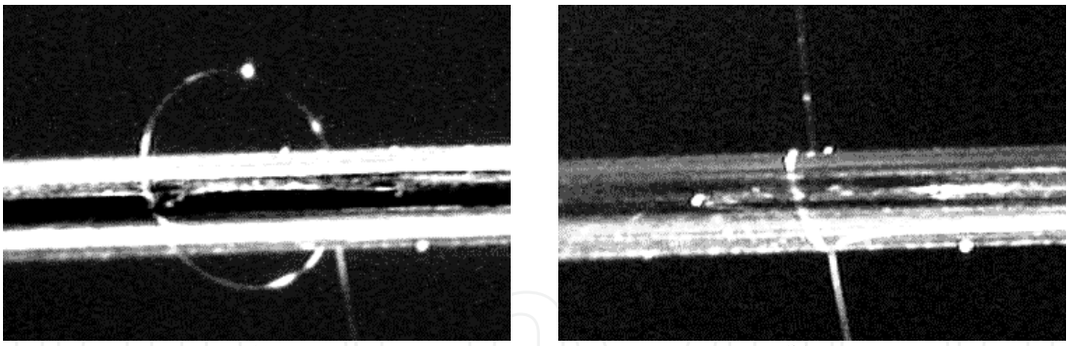

(a) (b)

Fig. 33. Optical microscope image of MKR tied on a copper wire.

The optical characteristics of the resonator are strongly affected by the tensile strain on the microfiber arms of the MKR induced by the pulling on the microfibers arms. It is essential to reduce the tension on the both arms of the MKR by moving the fiber holders a bit closer to the microfiber knot after the knot is fastened. In spite of that, there is a very little change at the knot diameter and the resonance condition of the MKR remains good and stable after the tension is released.

Theoretical Background

By wrapping microfiber on a current loaded conductor rod, the conductor rod acts as a heating element. It generates heat and increases the temperature of the microfiber. As

discussed earlier in Section 13, the transmission spectrum of a microfiber based device shifts as its ambient temperature varies and the relationship between these two variables is well described by the linear equation in Eqn. (26). Consider the linear relationship between the temperature change and heat energy generated by the conducting current, the relationship between wavelength shift and the conducting current, I can be expressed in the form of

$$\frac{\Delta\lambda_{res}}{\lambda_{res}} \propto \frac{\rho I^2}{A} \tag{27}$$

where ρ and A represent the conductor resistivity and the cross sectional area of the conductor rod, respectively. The term ρ / A in Eqn. (27) is equivalent to the resistance per unit length of the conductor material. The resistivity of the copper rod is 1.68×10^{-8} Ω·m.

Current Response

For optical characterization of the MKR, broadband source from amplified spontaneous emission is first launched into and guide along the SMF and then squeezed into the microfiber through the taper area. The light transmitted out from the MKR is collected by the collection fiber and measured by an OSA. The optical resonance is generated when light traversing the MKR. When an alternating current flows through the copper wire, heat is produced in the wire to change temperature. Because the MKR is in contact with the copper wire, any temperature changes will influence the refractive index and the optical path length of the MKR.

Fig. 34 shows the resonant spectral of the MKR tied on a copper wire with various current loadings. In the experiment, the applying current is uniformly increased from 0 to 2A.

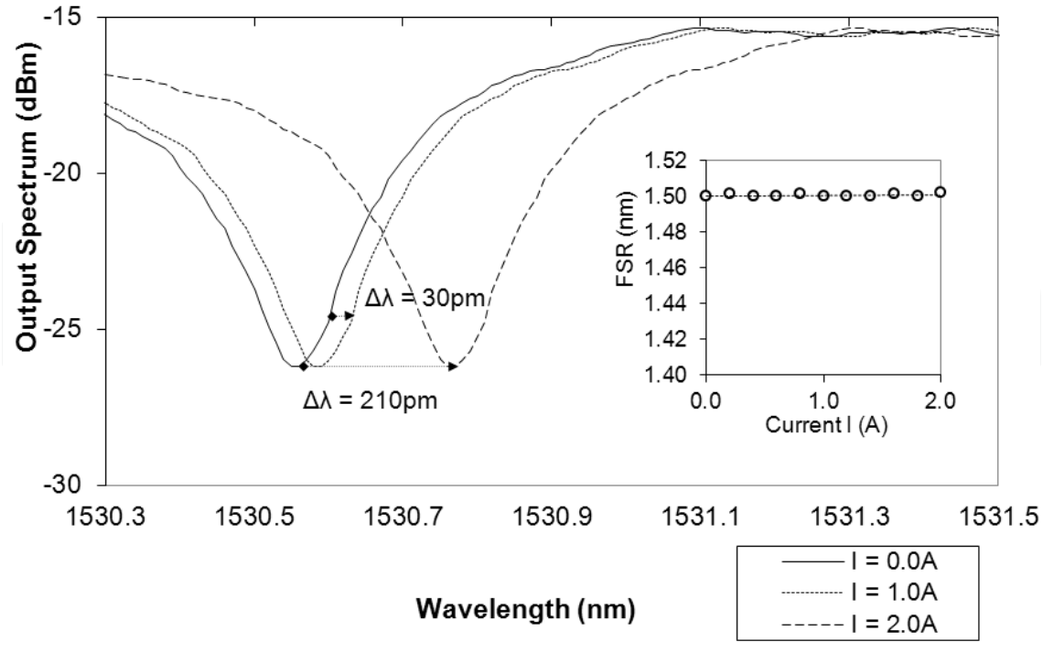

Fig. 34. Resonant wavelength shift of the MKR tied on a copper rod loaded with different current. Inset shows unchanged FSR with the increasing current.

In the spectrum, the resonant wavelength shifts to a longer wavelength the increasing of conducting current in the copper wire. The response time of the wavelength shift is approximately 3s and the spectrum comes to steady condition after 8s. Therefore, each spectrum is recorded at ~10s after the copper wire is loaded with an electric current. At loading current I = 1.0A, the resonant wavelength is shifted by ~30pm from 1530.56nm to 1530.59nm and at I = 2.0A, the resonant wavelength is further shifted to 1530.77nm, 210pm from the original wavelength. Inset of Fig. 34 shows the free spectral range of the transmitted spectrum against the applying currents. As shown in the inset, FSR of the MKR remains unchanged at 1.5 nm with the increasing current. The calculated Q factor and finesse of the MKR are ~4400 and 4.3 respectively. It is also observed that the transmission spectrum always shift towards the longer wavelength direction with increasing current regardless of the current flow direction, and the spectrum returns to original state once current supply is terminated.

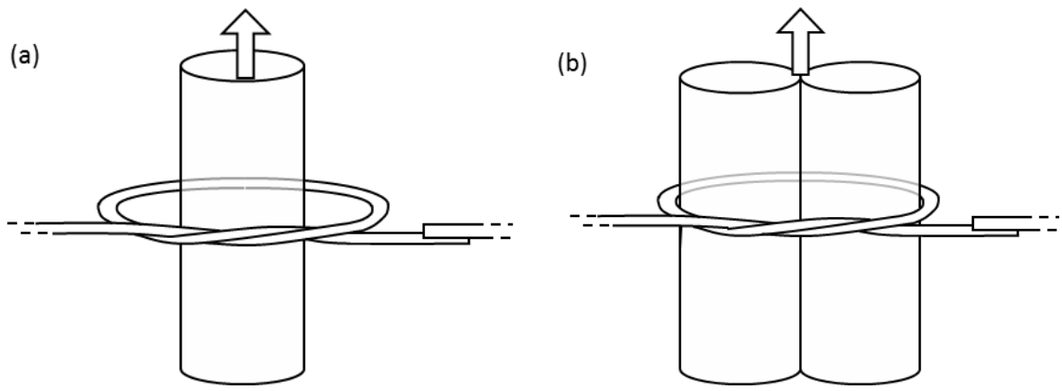

Fig. 35. Schematic illustrations of microfiber knot tied on (a) single copper wire (b) two copper wires with identical wire diameter of ~200μm.

Fig. 35(a) and Fig. 35(b) give schematic illustrations of MKR wrapped on a single copper rod and two copper rods respectively. The measured FSR and knot diameter of the single-rod MKR are 1.7nm and ~317μm respectively while for the two-rod MKR, the measured FSR and knot diameter are 1.46nm and ~370μm. An direct current is applied through the copper wire and the resonant wavelength shift is investigated against the applying current. At small current of < 0.5A, no significant resonant wavelength shift is observed. Beginning at 0.6A, the resonant wavelength shifts gradually toward the longer wavelength. At applying current of 2.0A, a wavelength shift of 0.208nm and 0.09nm are achieved with single and two copper wires configurations of Fig. 35(a) and Fig. 35(b), respectively. Fig. 36 shows the resonant wavelength shift against a square of current (I^2) for both configurations. The data set of each configuration can be well fit with a linear regression line with a correlation coefficient value r > 0.95. This justifies the linear relationship stated in Eqn. (27). In comparing the conductor wire cross-sectional area between the two configurations, the two-wire configuration is twice larger than the single-wire configuration. Based on the relation in Eqn. (27), the tuning slope of the wavelength shift with I^2 of the two-wire configuration should be a half of the single-wire configuration. The slope of each linear line is 51.3pm/A^2 (single rod) and 19.5pm/A^2 (two rods) nonetheless it is reasonable to attribute the mismatch between the analysis and experiment to the different orientation and position of the rod(s) in the MKR. The tuning slope of the current sensor can be further increased by using different

conductors with higher resistivity such as nichrome, constantan, graphite and etc which are commonly used as heating elements. However, the suitability in integration with microfiber or other opto-dielectric device remains uncertain.

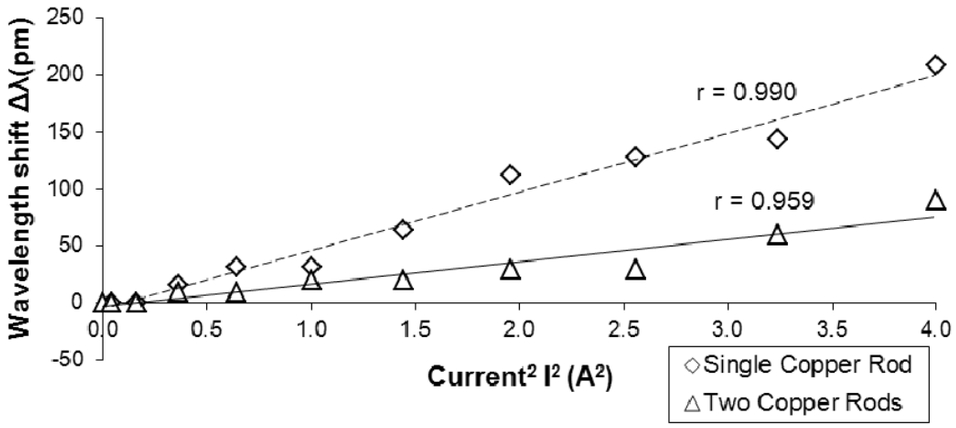

Fig. 36. Current response of MKRs based on single-wire and two-wire configurations. The calculated resistance of the single copper wire and two copper wire are 0.53 Ω·m^{-1} and 0.26Ω·m^{-1} respectively.

4.3. Microfiber Coil Resonator (MCR)

Microfiber coil resonators (MCRs) possess similar functionality with other microfiber resonators. It is useful for the applications of optical filtering, lasers and sensors. Additionally, it can be employed as an optical delay line for the optical communication network with small compactness. It is fabricated by winding a long microfiber on a low-index dielectric rod or a rod coated with low-index material (Sumetsky et al., 2010). The helical structure of microfiber coil enables propagation of light along the microfiber, across between the turns of microfiber in the forward and backward directions as illustrated in Fig. 37.

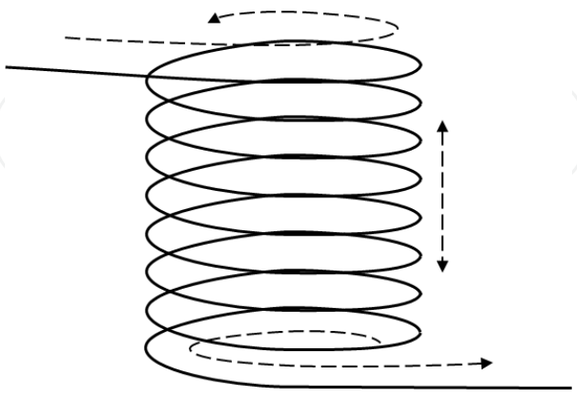

Fig. 37. Helical structure of an MCR and the propagation direction of the light in the resonator.

Fig. 38 shows the transmission spectra of an MCR of increasing number of microfiber turns. The microfiber was wound on a 0.5mm-diameter low-index coated rod. Basically, the optical

characteristics a 1-turn MCR is exactly identical to that of MLR, for instance the interference fringes in the MCR transmission spectrum are equally spaced as shown in Fig. 38(a). From the spectrum, the measured FSR is ~0.8nm and the estimated diameter of the coil is ~0.6mm which is slightly larger than the rod diameter. When making additional turns to the coil, it is important to ensure overlapping or touching between turns to establish coupling between them. For every additional turn is made, the transmission spectrum of the MCR is altered. Figs. 38(b)-(d) show the transmission spectra of a 2-turn, 3-turn and 4-turn MCR fabricated in the laboratory. Consider the elastic force from the bent microfiber; it is very difficult to maintain the resonance condition and increasing the number of turns at the same. With the assistance of microscope, the ensuing coiling work can be alleviated. Nonetheless, the reproducibility of MCR was difficult and tedious. Compared with the other microfiber resonators, MCRs have more complicated light propagation properties (Hsu and Huang, 2005).

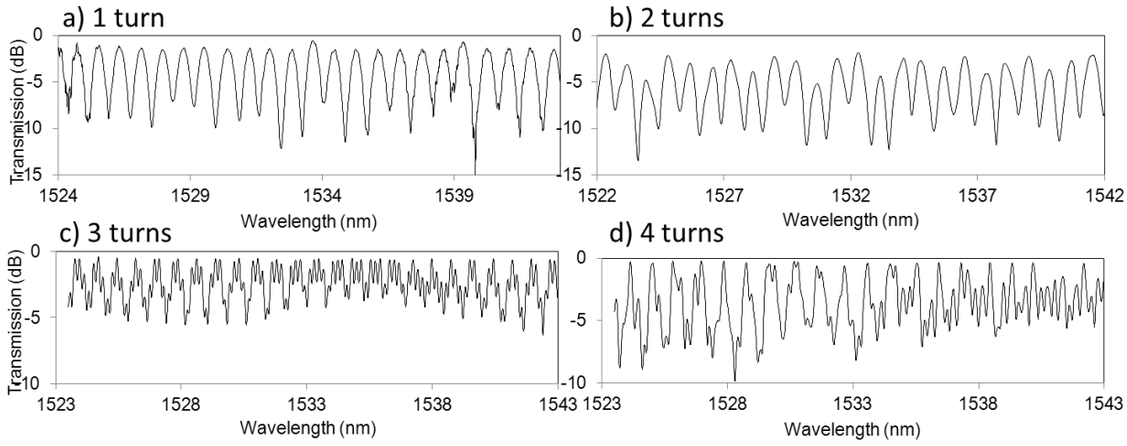

Fig. 38. Transmission spectra of a) 1 turn b) 2 turns c) 3 turns and d) 4 turns MCR.

5. Summary

In the past, several fabrication techniques for tapered fibers/microfibers have been suggested. In this chapter, fabrication of microfiber based on flame brushing technique is reviewed. Flame brushing technique is commonly used for the fabrication of fiber couplers and tapered fibers. This technique enables fabrication of biconical tapered fibers which are important components for the manufacture of microfiber based devices. In order to achieve that, a fiber tapering rig was assembled. The heat source comes from an oxy-butane torch with a flame width of 1mm. Two stepper motors are incorporated in the rig to control the movement of the torch and translation stage. A biconical tapered fiber with a waist diameter as small as 700nm can be achieved with the rig. To achieve low loss tapered fibers, the shape of the taper should be fabricated according to adiabaticity criteria. In the laboratory, tapered fibers with linear and decaying-exponential profiles have been demonstrated. To provide protection to the tapered fibers, they are embedded in a low-index material or packaged into a perspex case. These protection measures can prolong the life span and stabilize the temperal performance of these tapered fibers and microfiber based devices.

Three microfiber based devices have been reviewed in this chapter namely MLR, MKR and MMZI. In the first section, the fabrication of MLR is introduced. MLR is assembled from a

single mode microfiber by coiling it into a loop. A closed optical path within the loop is established when the two microfibers are put in close contact with each other and form an evanescent coupling. Then, the theoretical model of the self-touching MLR is presented and used for curve-fitting with the experimental data. The important characteristic parameters of the transmission spectra can be extracted from the best-fit curve in the experimental data. In the next section, MKR is presented. Similar to MLR, MKR shares the similar transmission characteristics and the same theoretical model for the MLR can be applied to MKR. However, MKR outperforms MLR in several aspects for instance MKR has more stable and stronger coupling due to its small spacing between the two coupling microfibers in the coupling region. In addition, the structure of MKR is more rigid and robust with the interfiber twisted coupling in the resonator. Nonetheless, MKRs suffer a setback in higher insertion loss if compared with MLRs because of the cut-coil-couple process in the fabrication. The evanescent coupling between output microfiber and collector microfiber contributes a large fraction in the total insertion loss. When MKR is embedded into a medium of different refractive index, the coupling in the MKR varies and it alters the resonance state of the resonator. By curving the experimental data for transmission spectra with the theoretical model, the coupling coefficient and round-trip attenuation factor of the MKR can be extracted from the best-fit curve. The results indicate that the state of resonance of an embedded MKR has been altered and it is closer to critical coupling condition.

Besides, microfiber based resonators exhibit an interesting polarization dependent characteristic in the investigation. The coupling coefficient in the resonator is dependent on input state of polarization and it can be manipulated by using a PBS and a PC. In relation with the coupling, the resonance extinction ratio (RER) of transmission spectrum can be varied by tuning the PC. In the experiment, the variation of RER between 5dB and 11dB was observed. In the past, several literatures have reviewed that the refractive index and dimension of silica microfiber have a strong dependence on temperature. The resonance extinction ratio and resonance wavelength can be expressed in functions of temperature. In order to gain insight into this characteristic, an investigation was conducted to study temperature response of an MKR. Both theoretical analysis and experimental result indicate that the spectral shift in the transmission of MKR is linearly proportional to the increment of temperature. This characteristic can be exploited in many applications particular in sector industrial sensors. By wrapping the microfiber knot on a conductor rod, MKR can perform as a current sensor. When an electric current is loaded through the conductor rod, the rod acts as a heating element and increases the temperature of the MKR. As a result, transmission spectrum of the MKR is shifted. This opto-electric configuration can be used a current sensor and an electric controlled optical filter. In the final section, the fabrication of MCR was demonstrated. An MCR of different number of turns was assembled and tested.

6. References

Bilodeau, F., K. O. Hill, S. Faucher, and D. C. Johnson, (1988), Low-loss highly overcoupled fused couplers: Fabrication and sensitivity to external pressure, *Lightwave Technology, Journal of* 6, 1476-1482.

Birks, T. A., and Y. W. Li, (1992), The shape of fiber tapers, *Lightwave Technology, Journal of* 10, 432-438.

Brambilla, G., F. Xu, and X. Feng, (2006), Fabrication of optical fibre nanowires and their optical and mechanical characterisation, *Electronics Letters* 42, 517-519.

Bricheno, T., and V. Baker, (1985), All-fibre polarisation splitter/combiner, *Electronics Letters* 21, 251-252.

Caspar, C., and E. J. Bachus, (1989), Fibre-optic micro-ring-resonator with 2 mm diameter, *Electronics Letters* 25, 1506-1508.

Chen, C.-L., and W. K. Burns, (1982), Polarization characteristics of single-mode fiber couplers, *Microwave Theory and Techniques, IEEE Transactions on* 30, 1577-1588.

Chen, Yi-Huai; Wu, Yu; Rao, Yun-Jiang; Deng, Qiang; Gong, Yuan, (2010), Hybrid mach-zehnder interferometer and knot resonator based on silica microfibers, *Optics Communications* 283, 4.

Ding, Lu, Cherif Belacel, Sara Ducci, Giuseppe Leo, and Ivan Favero, (2010), Ultralow loss single-mode silica tapers manufactured by a microheater, *Appl. Opt.* 49, 2441-2445.

Dong, H., G. Zhu, Q. Wang, H. Sun, N. K. Dutta, J. Jaques, and A. B. Piccirilli, (2005), Multiwavelength fiber ring laser source based on a delayed interferometer, *Photonics Technology Letters, IEEE* 17, 303-305.

Frazão, O., and et al., (2005), Chirped bragg grating fabricated in fused fibre taper for strain–temperature discrimination, *Measurement Science and Technology* 16, 984.

Graf, J. C., S. A. Teston, P. V. de Barba, J. Dallmann, J. A. S. Lima, H. J. Kalinowski, and A. S. Paterno, 2009, Fiber taper rig using a simplified heat source and the flame-brush technique, Microwave and Optoelectronics Conference (IMOC), 2009 SBMO/IEEE MTT-S International.

Guo, Xin, Yuhang Li, Xiaoshun Jiang, and Limin Tong, (2007), Demonstration of critical coupling in microfiber loops wrapped around a copper rod, *Applied Physics Letters* 91, 073512-3.

Guo, Xin, and Limin Tong, (2008), Supported microfiber loops for optical sensing, *Opt. Express* 16, 14429-14434.

Harun, S., K. Lim, A. Jasim, and H. Ahmad, (2010), Fabrication of tapered fiber based ring resonator, *Laser Physics* 20, 1629-1631.

Harun, S. W., K. S. Lim, A. A. Jasim, and H. Ahmad, (2010), Dual wavelength erbium-doped fiber laser using a tapered fiber, *Journal of Modern Optics* 57, 2111 - 2113.

Hou, Changlun, Yu Wu, Xu Zeng, Shuangshuang Zhao, Qiaofen Zhou, and Guoguang Yang, (2010), Novel high sensitivity accelerometer based on a microfiber loop resonator, *Optical Engineering* 49, 014402-6.

Hsu, Shih-Hsin, and Yang-Tung Huang, (2005), Design and analysis of mach?Zehnder interferometer sensors based on dual strip antiresonant reflecting optical waveguide structures, *Opt. Lett.* 30, 2897-2899.

Jiang, Xiaoshun, Limin Tong, Guillaume Vienne, Xin Guo, Albert Tsao, Qing Yang, and Deren Yang, (2006), Demonstration of optical microfiber knot resonators, *Applied Physics Letters* 88, 223501-223501-3.

Jung, Y, G. S. Murugan, G. Brambilla, and D. J. Richardson, (2010), Embedded optical microfiber coil resonator with enhanced high-q, *Photonics Technology Letters, IEEE* 22, 1638-1640.

Li, Yuhang, and Limin Tong, (2008), Mach-zehnder interferometers assembled with optical microfibers or nanofibers, *Opt. Lett.* 33, 303-305.

Lim, K. S., S. W. Harun, S. S. A. Damanhuri, A. A. Jasim, C. K. Tio, and H. Ahmad, (2011), Current sensor based on microfiber knot resonator, *Sensors and Actuators A: Physical* 167, 377–381.

Lim, K. S., S. W. Harun, A. A. Jasim, and H. Ahmad, (2011), Fabrication of microfiber loop resonator-based comb filter, *Microwave and Optical Technology Letters* 53, 1119-1121.

Liu, Zhihai, Chengkai Guo, Jun Yang, and Libo Yuan, (2006), Tapered fiber optical tweezers for microscopic particle trapping: Fabrication and application, *Opt. Express* 14, 12510-12516.

Love, J. D., W. M. Henry, W. J. Stewart, R. J. Black, S. Lacroix, and F. Gonthier, (1991), Tapered single-mode fibres and devices. I. Adiabaticity criteria, *Optoelectronics, IEE Proceedings J* 138, 343-354.

Mora, J., A. Diez, M. V. Andres, P. Y. Fonjallaz, and M. Popov, (2004), Tunable dispersion compensator based on a fiber bragg grating written in a tapered fiber, *Photonics Technology Letters, IEEE* 16, 2631-2633.

Ngo, N. Q., S. Y. Li, R. T. Zheng, S. C. Tjin, and P. Shum, (2003), Electrically tunable dispersion compensator with fixed center wavelength using fiber bragg grating, *Lightwave Technology, Journal of* 21, 1568-1575.

Orucevic, Fedja, Valérie Lefèvre-Seguin, and Jean Hare, (2007), Transmittance and near-field characterization of sub-wavelength tapered optical fibers, *Opt. Express* 15, 13624-13629.

Schwelb, O., (2004), Transmission, group delay, and dispersion in single-ring optical resonators and add/drop filters-a tutorial overview, *Lightwave Technology, Journal of* 22, 1380-1394.

Sumetsky, M., (2008), Basic elements for microfiber photonics: Micro/nanofibers and microfiber coil resonators, *J. Lightwave Technol.* 26, 21-27.

Sumetsky, M., Y. Dulashko, J. M. Fini, and A. Hale, (2005), Optical microfiber loop resonator, *Applied Physics Letters* 86, 161108-161108-3.

Sumetsky, M., Y. Dulashko, J. M. Fini, A. Hale, and D. J. DiGiovanni, (2006), The microfiber loop resonator: Theory, experiment, and application, *Lightwave Technology, Journal of* 24, 242-250.

Sumetsky, M., Y. Dulashko, and S. Ghalmi, (2010), Fabrication of miniature optical fiber and microfiber coils, *Optics and Lasers in Engineering* 48, 272-275.

Tong, Limin, Rafael R. Gattass, Jonathan B. Ashcom, Sailing He, Jingyi Lou, Mengyan Shen, Iva Maxwell, and Eric Mazur, (2003), Subwavelength-diameter silica wires for low-loss optical wave guiding, *Nature* 426, 816-819.

Vienne, G., Li Yuhang, and Tong Limin, (2007), Effect of host polymer on microfiber resonator, *Photonics Technology Letters, IEEE* 19, 1386-1388.

Vienne, Guillaume, Aurélien Coillet, Philippe Grelu, Mohammed El Amraoui, Jean-Charles Jules, Frédéric Smektala, and Limin Tong, (2009), Demonstration of a reef knot microfiber resonator, *Opt. Express* 17, 6224-6229.

Wu, Yu, Yun-Jiang Rao, Yi-huai Chen, and Yuan Gong, (2009), Miniature fiber-optic temperature sensors based on silica/polymer microfiber knot resonators, *Opt. Express* 17, 18142-18147.

Xu, Fei, and Gilberto Brambilla, (2007), Embedding optical microfiber coil resonators in teflon, *Opt. Lett.* 32, 2164-2166.

Xu, Fei, Gilberto Brambilla, and David J. Richardson, 2006, Adiabatic snom tips for optical tweezers.

Xu, Fei, Peter Horak, and Gilberto Brambilla, (2007), Optical microfiber coil resonator refractometric sensor, *Opt. Express* 15, 7888-7893.

Xu, Fei, Valerio Pruneri, Vittoria Finazzi, and Gilberto Brambilla, (2008), An embedded optical nanowire loop resonator refractometric sensor, *Opt. Express* 16, 1062-1067.

Yang, Szu-Wen, and Hung-Chun Chang, (1998), Numerical modeling of weakly fused fiber-optic polarization beamsplitters. I. Accurate calculation of coupling coefficients and form birefringence, *Lightwave Technology, Journal of* 16, 685-690.

Zeng, Xu, Yu Wu, Changlun Hou, Jian Bai, and Guoguang Yang, (2009), A temperature sensor based on optical microfiber knot resonator, *Optics Communications* 282, 3817-3819.

Zhang, J., P. Shum, X. P. Cheng, N. Q. Ngo, and S. Y. Li, (2003), Analysis of linearly tapered fiber bragg grating for dispersion slope compensation, *Photonics Technology Letters, IEEE* 15, 1389-1391.

Zhang, Rui, Jörn Teipel, Xinping Zhang, Dietmar Nau, and Harald Giessen, (2004), Group velocity dispersion of tapered fibers immersed in different liquids, *Opt. Express* 12, 1700-1707.

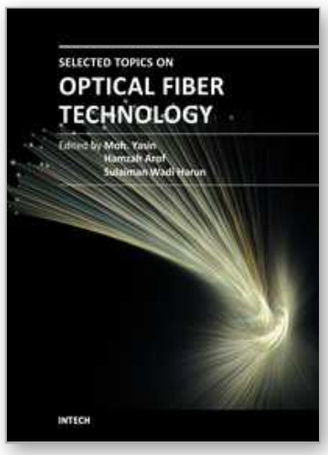

Selected Topics on Optical Fiber Technology

Edited by Dr Moh. Yasin

ISBN 978-953-51-0091-1

Hard cover, 668 pages

Publisher InTech

Published online 22, February, 2012

Published in print edition February, 2012

This book presents a comprehensive account of the recent advances and research in optical fiber technology. It covers a broad spectrum of topics in special areas of optical fiber technology. The book highlights the development of fiber lasers, optical fiber applications in medical, imaging, spectroscopy and measurement, new optical fibers and sensors. This is an essential reference for researchers working in optical fiber researches and for industrial users who need to be aware of current developments in fiber lasers, sensors and other optical fiber applications.

How to reference

In order to correctly reference this scholarly work, feel free to copy and paste the following:

K. S. Lim, S. W. Harun, H. Arof and H. Ahmad (2012). Fabrication and Applications of Microfiber, Selected Topics on Optical Fiber Technology, Dr Moh. Yasin (Ed.), ISBN: 978-953-51-0091-1, InTech, Available from: http://www.intechopen.com/books/selected-topics-on-optical-fiber-technology/fabrication-and-applications-of-microfiber

INTECH
open science | open minds

InTech Europe
University Campus STeP Ri
Slavka Krautzeka 83/A
51000 Rijeka, Croatia
Phone: +385 (51) 770 447
Fax: +385 (51) 686 166
www.intechopen.com

InTech China
Unit 405, Office Block, Hotel Equatorial Shanghai
No.65, Yan An Road (West), Shanghai, 200040, China
中国上海市延安西路65号上海国际贵都大饭店办公楼405单元
Phone: +86-21-62489820
Fax: +86-21-62489821

IntechOpen